Int J Clin Exp Med 2026;19(4):101-115
www.ijcem.com /ISSN:1940-5901/IJCEM0166567

Original Article

Study on the mechanism of Qingre Yangyin Chushi Decoction (QYCD) against rheumatoid arthritis based on network pharmacology

Jing Zhang[1*], Lu Liu[2*], Jie Fan[1], Yang-Li Zhang[1], Mi-Feng Liu[1]

[1]Beijing Hospital of Traditional Chinese Medicine, Capital Medical University, Beijing 100010, China; [2]Guang'anmen Hospital, China Academy of Chinese Medical Sciences, Beijing 100032, China. [*]Equal contributors and co-first authors.

Received June 4, 2025; Accepted March 19, 2026; Epub April 15, 2026; Published April 30, 2026

Abstract: Objective: Qingre Yangyin Chushi Decoction (QYCD) is an effective clinically empirical prescription widely used in the treatment of various rheumatic diseases. This study aims to explore the mechanism of action of QYCD on joint injury in collagen-induced arthritis (CIA) model rats using network pharmacology methods. Methods: A rat model of collagen-induced arthritis was established based on literature data. Hematoxylin-Eosin (HE) staining and micro-computed tomography (micro-CT) scanning were used to observe the pathological morphological changes and microstructure of the ankle joints in rats. Enzyme-linked immunosorbent assay (ELISA) was used to measure the levels of serum inflammatory factors and bone injury indicators. The GeneCards database was used to search and predict RA-related targets, and overlapping targets between drugs and diseases were analyzed based on GEO chip transcriptional disease target prediction. Network pharmacology techniques were used to screen the potential core active components of QYCD, and molecular docking technology was employed to verify the identified core targets and candidate compounds, aiming to explore the potential mechanism of QYCD in treating rheumatoid arthritis (RA). Results: QYCD alleviated inflammatory cell infiltration and cartilage surface erosion in CIA rats. QYCD reduced the levels of pro-inflammatory cytokines IFN-γ and IL-17A in CIA rats, while increasing the levels of anti-inflammatory cytokines IL-4 and TGF-β. Through network pharmacology screening, nine candidate compounds were identified. By analyzing the intersections of drugs, diseases, and transcriptional targets, seven core targets were determined, namely COL1A1, LDLR, VEGFA, MYC, MCL1, EGFR, and FOSL2, which are involved in the EGFR, HIF-1, VEGF, and PI3K-AKT signaling pathways. The results of molecular docking analysis indicated that most compounds exhibited strong binding interactions with target proteins, indicating strong binding affinity (binding energy less than -6 kcal/mol). Conclusion: These compounds can form stable complexes with proteins and are potential active compounds for the treatment of RA.

Keywords: Qingre Yangyin Chushi Decoction (QYCD), Collagen Induced Arthritis (CIA), cytokine, network pharmacology

Introduction

Rheumatoid arthritis (RA) is a common, systemic autoimmune disease. It has pathological features of invasive synovitis, formation of vascular opacities, and destruction of articular cartilage, which can lead to progressive joint destruction. Musculoskeletal pain, swelling, and stiffness are the common clinical manifestations of RA. In addition to the affected joints, patients with RA have extra-articular manifestations, often accompanied by related cardiovascular, pulmonary, gastrointestinal, metabolic, skeletal, and psychological complications [1-3]. The average prevalence of RA worldwide is 0.5%-1% [4], and its pathogenesis is not fully understood. Genetic susceptibility, infection, environmental factors, and immune abnormalities are closely associated with RA pathogenesis [5]. Antirheumatic drugs (DMARDs), nonsteroidal anti-inflammatory drugs, glucocorticoids, and immunosuppressants that improve the condition are common therapeutic drugs used for patients with RA [6]. Methotrexate (MTX) remains one of the most widely used DMARDs, but studies have shown that the response rate

https://doi.org/10.62347/UUKK6693

to MTX monotherapy is generally low [7, 8]. Despite the availability of numerous RA treatment drugs, a considerable number of patients with RA do not respond to current treatment strategies [9] and may even experience long-term adverse reactions such as gastrointestinal toxicity, hepatotoxicity, bone marrow suppression, tuberculosis, and infection [10]. Therefore, finding new, effective, and safe treatment strategies remains the focus of the current research.

RA belongs to the category of "arthralgia syndrome" in traditional Chinese medicine (TCM). Arthralgia syndrome has been described in detail in the ancient TCM literature. For instance, Zheng-Zhi Zhun-Sheng recorded that "wind, damp, cold, and heat are superficial causes of arthralgia, and kidney deficiency plays a fundamental role in causing RA. The etiology of RA is mainly attributed to the deficiency of Qi and blood, combined with external invasions by the pathogenic factors of wind, cold, dampness, and heat, resulting in the mutual binding of phlegm and blood stasis. Furthermore, constitutional vacuity and deficiency of vital Qi are considered internal causes. Based on internal causes, the body is more vulnerable to attack by wind, cold, dampness, heat, and other pathogenic factors, leading to obstruction of meridians and collaterals and blocking of Qi and blood circulation. TCM has a long history of treating RA, and its efficacy and safety have been inferred from clinical experience and verified in clinical trials [11, 12]. TCM has outstanding advantages in reducing drug side effects, alleviating local pain, and improving the physical status of patients with RA, and its clinical application has broad prospects. QYCD is a clinically effective prescription commonly used at Beijing Traditional Chinese Medicine Hospital affiliated to Capital Medical University for decades to treat RA. However, its pharmacodynamic mechanism remains unclear. This study used a rat model of CIA and network pharmacological methods to preliminarily explore the potential active components, related targets, and molecular signaling pathways of QYCD, as well as the efficacy and possible mechanism of QYCD in the treatment of RA, to provide a theoretical basis for the effectiveness of the integrated treatment of traditional Chinese and Western medicine.

Material and methods

Drugs and reagents

Incomplete Freund's adjuvant (IFA, 7002) and bovine collagen type II (CII, 20022) were provided by Chondrex, Inc. (WA, USA). MTX tablets (National Yaozhun: H31020644) were purchased from Shanghai Xin Yi Pharmaceutical Co. Ltd. (Shanghai, China). Enzyme-linked immunosorbent assay (ELISA) kits for TGF-β (DG20110D), IFN-γ (DG20066D), IL-4 (DG-94488Q), IL-17 (DG94480Q), tartrate resistant acid phosphatase (TRAP, DG20097D), receptor activator for nuclear factor-κB ligand (RANKL) (DG20545D), and OPG (DG20656D) were purchased from Beijing Winter Song Boye Biotechnology Co., Ltd (Beijing, China).

Preparation of QYCD

The following herbs were tested using the QYCD formula from Beijing Xinglin Pharmaceutical Co., Ltd.: Hedyotis diffusa Willd, Lonicera japonica Thunb, Forsythia suspensa, Sculellaria barbata, Rhizoma Polygoni Cusp, Radix Rehmanniae, Cortex dictamni, Cassia twig, Honeysuckle vine, Cortex moutan, Radix Rehmanniae Praeparata, and Paeoniae Radix Alba (report numbers: C20190627-01, C20190326-02, C2018-1228-01, C20190725-01, C20190703-04, C20190723-01, C20190312-02, C20190530-02, C20190412-01, C201908 517-15, C2019-0611-09, C20190731-02). The Radix Aconiti Preparata (report number: DX-C2019081901) was tested by Beijing Huamiao Pharmaceutical Co., Ltd.The Rhizoma smilacis glabrae (report number: C201805023) was tested by Beijing Taiyang Shukang Traditional Chinese Medicine Herbal Pieces Factory. All procedures conformed to the standards of the Chinese Pharmacopoeia (2015 edition). QYCD was uniformly prepared by the Formulation Department of Beijing Traditional Chinese Medicine Hospital Affiliated to Capital Medical University.

Induction and evaluation of CIA

This study selected female Wistar rats aged 6-7 weeks, purchased from Huafukang Company in Beijing, China (animal license number: SCXK Jing 2019-0010). During the experimental stage, the age of the rats was 7-8 weeks old. They had free access to commercial feed and tap water. The animal experimental protocol

of this study was approved by the Animal Ethics Committee of Beijing Traditional Chinese Medicine Hospital, Capital Medical University (Approval No. 2019100102; Beijing, China). All animal husbandry and experiments were conducted in strict accordance with the standards in the Guidelines for Laboratory Animal Care and Use of the National Institutes of Health (NIH). As mentioned earlier, CIA was induced in rats [13]. On the seventh day after sensitization, the degree of joint disease in the limbs of rats was observed and evaluated for the arthritis index once a week. A five-point scoring system was used to calculate the arthritis index based on the cumulative score of disease severity [13]. The arthritis index of each rat was calculated as the sum of its limbs. The normal control group was injected with the same volume of physiological saline at the same site. After 14 days of initial immunization, experimental animals with an arthritis index (AI) ≥ 4 were considered successfully modeled.

Experimental protocols

On the 14th day after the initial immunization, CIA modeled rats were randomly divided into the following groups: model (CIA), methotrexate (MTX), and QYCD, with six animals in each group. In addition, a normal (control) group was established. The MTX group was treated with a 0.625 mg/kg clinically equivalent dose twice a week, the QYCD group was treated with a clinically equivalent dose of 17 g/kg once a day, and the control and CIA groups were administered 0.9% normal saline once a day. All doses were intragastrically administered at a volume of 10 mL/kg. The experimental drug doses were converted into equivalent doses based on the rat body surface area. After five weeks of drug intervention, the rats were fasted for eight hours (with free access to drinking) and then anesthetized by intraperitoneal injection of 1% sodium pentobarbital solution. Serum was collected through the abdominal aorta, followed by dissection of organs and hindpaws, which were then fixed with 4% paraformaldehyde for histological examination. To alleviate pain and distress, we provided appropriate anesthetics before and during the experiments. Regarding euthanasia, we adhered to established protocols to ensure a humane and ethically compliant procedures. Specifically, euthanasia was performed via intraperitoneal injection of an excessive dose of sodium pentobarbital (150 mg/kg) to guarantee rapid and painless death.

Histological examination

For histopathological analysis, hind paws were fixed in 4% paraformaldehyde and decalcified in 10% ethylenediaminetetraacetic acid for four weeks for ethanol gradient dehydration (from low to high). Xylene was used for transparency and the samples were embedded in paraffin. A tissue microtome was used to prepare 5 μm-thick paraffin sections, which were dewaxed with xylene, rehydrated with a gradient of ethanol (from high to low), and finally stained with hematoxylin and eosin (HE) to observe synovial hyperplasia, inflammatory infiltration, and neovascularization of joints. Histopathologic scoring was performed by examining the whole section and calculating the average score of all examination areas using the following grading system [14].

Micro-CT imaging of ankle joints

The morphometric indices of the joints were determined using micro-computed tomography (CT). The ankle joint was placed in a micro-CT test tube and scanned along the long axis of the specimen to obtain continuous images. The micro-CT (Bruker, Belgium) scanning parameters used were: image matrix 4096 × 4096, layer spacing 28.6 μm, source voltage 70 kV, current 400 μA, scanning time 432 s, and scanning rotated within 360°. After the micro-CT scan, reconstruction was performed, and the three-dimensional images of rat bones were obtained by threshold segmentation and saved. The software that was used with the micro-CT scanner was used for quantitative analysis to evaluate the differences in bone damage and bone morphological parameters in each group.

Cytokine and bone metabolism measurements

The levels of inflammatory factors IL-4, IL-17, IFN-γ, TGF-β, and bone injury indicators TRAP, RANKL, and OPG in peripheral blood were analyzed using commercially available Enzyme-Linked Immunosorbent Assay (ELISA) kits, according to the manufacturer's instructions. The highest detected concentrations of IL-4, IL-17, IFN-γ, TGF-β, TRAP, RANKL, and OPG were 120, 48, 2,000, 240, 48, 48, and 4,000 pg/mL, respectively. The absorbance wavelength

at 450 nm was read, and a standard curve was used to calculate the serum concentration.

Network pharmacology analysis

In 1998, the hospital optimized and developed a formula for QYCD into an in-house preparation, which was made into convenient pills, which is widely used for the treatment of various active rheumatic diseases. The main active components of QYCD were predicted through the TCMSP database under the conditions of oral bioavailability (OB) ≥ 30% and drug-likeness (DL) ≥ 0.18. The Gene Symbols of predicted targets were obtained using the VLOOKUP function of the UniProt database (https://www.uniprot.org/). The drug-active ingredient-target network diagram was constructed using Cytoscape 3.9.1 software, and network topology analysis was performed using the NetworkAnalyzer function of Cytoscape software. Based on the node degree values, the relevant network parameters of the main active ingredients of the drug and protein targets were screened to determine the possible core active ingredients of QYCD.

The GeneCards database (https://www.genecards.org), PharmGkb database (https://www.pharmgkb.org/), DisGeNET (https://www.disgenet.org/), and OMIM database (https://omim.org/) were utilized to search and predict RA-related targets. Disease-target prediction of RA based on transcriptomics from the GEO database of NCBI. The differential genes of chip data were analyzed using the limma package included in GEO2R, with adjusted $P < 0.05$, and |logFC| > 1.0 as the screening criteria. To clarify the interaction between drugs and potential targets of RA, the intersection targets between drug targets and disease targets were displayed in the form of a Venn diagram. Gene ontology (GO) functional enrichment analysis of common targets between diseases and drugs was performed using the DAVID 6.8 database (http://david.ncifcrf.gov/home.jsp). Based on KEGG pathway enrichment analysis, a bubble chart was drawn, and the signaling pathway network in the KEGG pathway enrichment analysis was further screened using Cytoscape3.9.1 to identify signaling pathways related to RA and to explore the biological processes and signaling pathways of QYCD against RA.

Molecular docking validation

The crystal structures of the seven core targets identified by network pharmacology, namely COL1A1 (PDB ID: 7E7B), EGFR (PDB ID: 5GNK), FOSL2 (PDB ID: P15408), LDLR (PDB ID: 1IJQ), MCL1 (PDB ID: 8G3S), MYC (PDB ID: 6E16), and VEGFA (PDB ID: 4GLS), were sourced from the Protein Data Bank (https://www.rcsb.org/). Nine candidate compounds (MOL000006, MOL000098, MOL000173, MOL000497, MOL000546, MOL001002, MOL002714, MOL002773, MOL004328) were obtained from the PubChem database (https://pubchem.ncbi.nlm.nih.gov/). The processed compounds were used as small-molecule ligands and seven protein targets were used as receptors. The center position and dimensions of the Grid Box, determined by the interaction between the small molecule and target, were set to 60 × 60 × 60. Finally, batch molecular docking was performed using AutoDock, and the results of the molecular docking were analyzed. Binding interactions between the compounds and proteins were visualized using Pymol2.1 software.

Statistical analysis

Data analysis was conducted utilizing the SPSS software version 24.0 (IBM Corp., Armonk, NY, USA). The findings are presented as means ± standard deviation (SD) and subjected to one-way analysis of variance (ANOVA), accompanied by the Bonferroni test or Tamhane's test. For data exhibiting a non-normal distribution, independent multi-sample nonparametric Kruskal-Wallis rank-sum tests were employed. Statistically significant differences between groups were identified at two thresholds: $P < 0.05$ and $P < 0.01$.

Results

Pathological and microstructural changes

Histological examination of the ankle joint showed that the surface of the ankle joint in the Control group was covered by a thin layer of transparent cartilage, the joint capsule cavity was smooth, and the synovial structure was clear, with no hyperplasia observed. In all CIA rats, the joint surface showed local disappearance of hyaline cartilage, replaced by fibrous connective tissue, the subchondral tra-

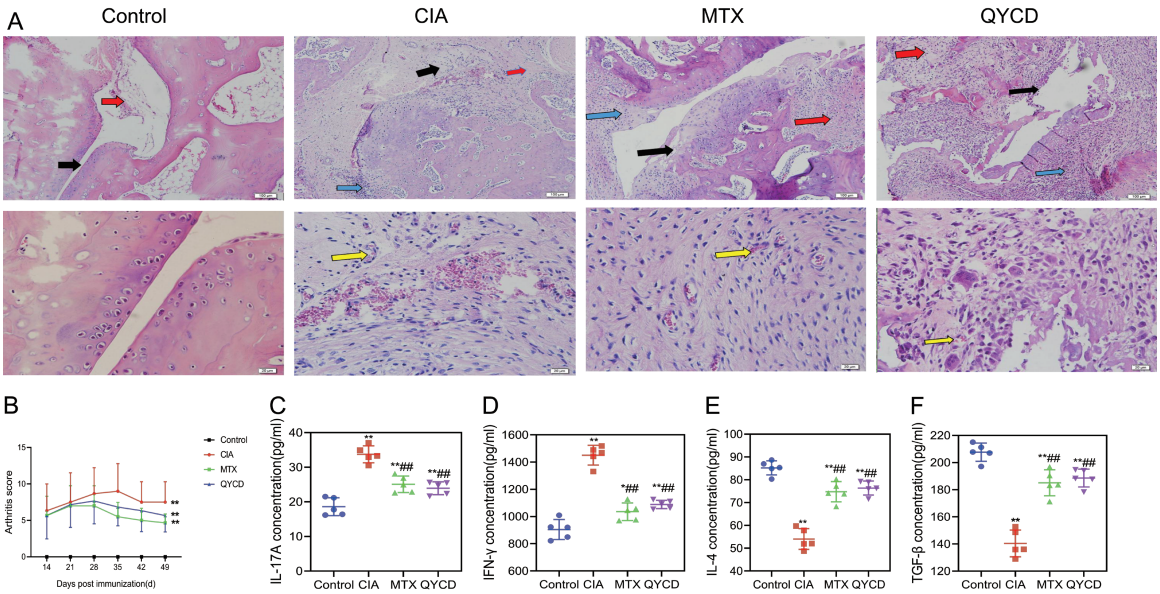

Figure 1. The effect of QYCD on the pathological morphology and inflammatory factors of joint tissue. A. Ankle joint histomorphology (HE staining, ruler: 100 μm and 20 μm). As indicated by the black arrow, in the control group, there is normal transparent cartilage, while in the CIA group, there is fibrous connective tissue that replaces transparent cartilage. The red arrow indicates that the subchondral trabecular bone is occupied by fibrous connective tissue, becoming thinner and sparser. The blue arrow indicates synovial thickening, accompanied by a large amount of inflammatory cell infiltration. The yellow arrow indicates connective tissue hyperplasia and angiogenesis. B. Arthritis index (AI) score. C-F. Serum levels of inflammatory factors IL-17A, IFN-γ, IL-4 and TGF-B. $**P < 0.01$, versus Control group; $\#P < 0.05$, $\#\#P < 0.01$, versus CIA group.

becular bone was occupied by fibrous connective tissue, becoming increasingly sparse and thin, the synovial membrane was significantly thickened, accompanied by a large number of inflammatory cell infiltrations, connective tissue hyperplasia, and a large amount of angiogenesis was observed, with the joint capsule cavity narrowing. The histological examination results of each treatment group were basically the same, with only some differences in severity (**Figure 1A**, **1B**). Compared to the control group, the levels of the anti-inflammatory factors TGF-β and IL-4 in the serum of rats in the CIA group were significantly decreased ($P < 0.01$), whereas the levels of the pro-inflammatory factors IFN-γ and IL-17A were significantly increased ($P < 0.01$). Compared with the CIA group, the intervention of the positive drugs MTX and QYCD significantly increased the levels of serum anti-inflammatory factors TGF-β and IL-4 ($P < 0.01$), and reduced the levels of pro-inflammatory factors IFN-γ and IL-17A ($P < 0.01$) (**Figure 1C-F**).

Micro-CT scanning showed that CIA rats had severe cartilage and bone destruction, with rough joint surfaces and significant bone erosion compared to the control group. MTX has a good protective effect, with the lowest degree of joint damage. QYCD had a certain protective effect, with the degree of bone damage in rats alleviated to a certain extent, and the joints were relatively intact, with only slight bone loss. This suggests that QYCD has a protective effect against joint damage in CIA modeled animals (**Figure 2A**). In addition, an analysis of the differences in bone mineral density (BMD) among the groups of rats showed that CIA rats had significantly lower BMD compared to the control group, and QYCD intervention could increase the BMD of CIA rats, but it still remained lower than that of the control group (**Figure 2B**). The expression of TRAP, RANKL, and OPG in the serum was detected by ELISA (**Figure 2C-E**). Compared with the control group, the serum TRAP and RANKL levels were increased in CIA rats, while the OPG level was decreased ($P < 0.01$). QYCD treatment reduced the levels of TRAP and RANKL, and increased the level of OPG ($P < 0.05$).

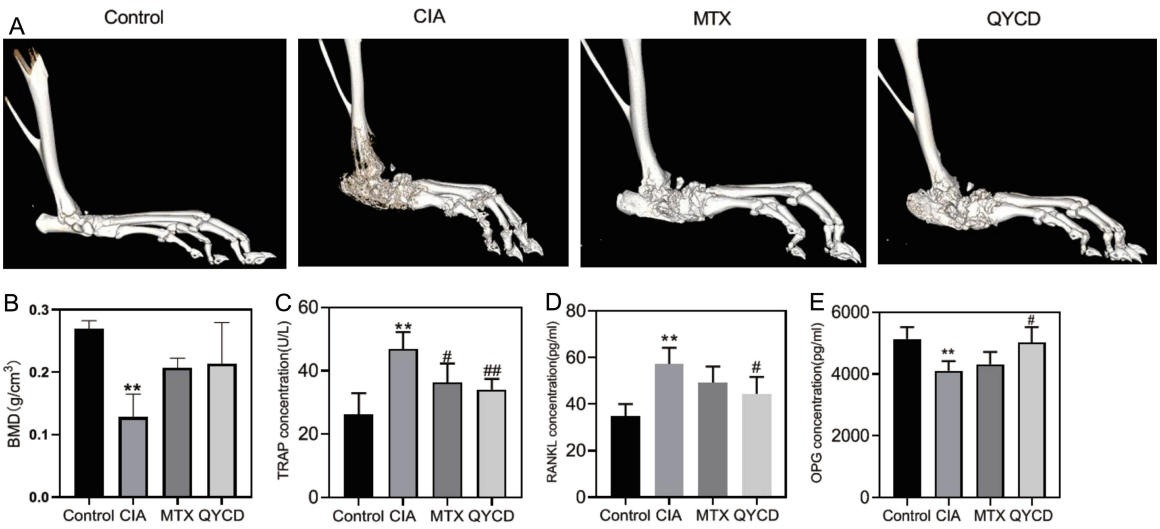

Figure 2. Effects of QYCD on bone destruction. A. Micro-CT images of the right foot of rats. B. Bone mineral density (BMD) analyzed by Micro-CT. C-E. Serum TRAP, RANKL, and OPG levels in rats. $^{**}P < 0.01$, versus Control group; $^{\#}P < 0.05$, $^{\#\#}P < 0.01$, versus CIA group.

Network pharmacology analysis

The number of active ingredients in the compound formula is as follows: 10 from Rhizoma Polygoni Cusp, 23 from Lonicera japonica Thunb, 23 from Forsythia suspensa, 15 from Rhizoma smilacis glabrae, 18 from Cortex dictamni, 3 from Radix Stephaniae Tetrandrae, 13 from Paeoniae Radix Alba, 3 from Radix Aconiti Preparata, 7 from Cassia twig, 92 from Radix glycyrrhizae, 7 from Hedyotis diffusa Willd, 11 from Cortex moutan, 29 from Radix paeoniae rubrathe, and 2 from Angelicae Pubescentis Radix. Using the Related Targets database in TCMSP, we predicted the target proteins corresponding to 205 small-molecule components of the aforementioned traditional Chinese medicines (Supplementary Table 1). Of these, 164 small molecules were found to have target proteins: 16 Rhizoma Polygoni Cusp, 17 Lonicera japonica Thunb, 19 Forsythia suspensa, 15 Rhizoma smilacis glabrae, 11 Cortex dictamni, 2 Radix Stephaniae Tetrandrae, 8 Paeoniae Radix Alba, 2 Radix Aconiti Preparata, 6 Cassia twig, 88 Radix glycyrrhizae, 5 Hedyotis diffusa Willd, 6 Cortex moutan, 14 Radix Paeoniae Rubrathe, and 2 Angelicae Pubescentis Radix. No relevant components of Radix rehmanniae were retrieved from the TCMSP database. Based on the retrieved literature, we directly obtained seven relevant targets. Subsequently, we converted the names of target proteins into their corresponding Gene Symbols using the UniProt database. The results showed 196 effective component targets for Rhizoma Polygoni Cusp, 214 for Lonicera japonica Thunb, 221 for Forsythia suspensa, 207 for Rhizoma smilacis glabrae, 198 for Cortex dictamni, 39 for Radix Stephaniae Tetrandrae, 91 for Paeoniae Radix Alba, 5 for Radix Aconiti Preparata, 51 for Cassia twig, 229 for Radix Glycyrrhizae, 185 for Hedyotis diffusa Willd, 168 for Cortex moutan, 98 for Radix Paeoniae rubrathe, 52 for Angelicae Pubescentis Radix, and 7 for Radix Rehmanniae. After removing duplicate targets, there were a total of 294 possible target proteins for this formula. Using Cytoscape 3.9.1 software for mapping, a drug-small-molecule component-target network diagram was obtained (since the direct target of Radix Rehmanniae was obtained, its small-molecule component-target network diagram has not yet been created). The results are shown in **Figure 3A**.

Using rheumatoid arthritis as the keyword, we searched and predicted RA-related targets using the Genecards, OMIM, and DisGeNET databases. We also conducted transcriptomic disease-target predictions based on the GEO database. The original chip data file, numbered GSE55457, was downloaded from the GEO database of NCBI. According to the annotation, this file contained 33 synovial samples, includ-

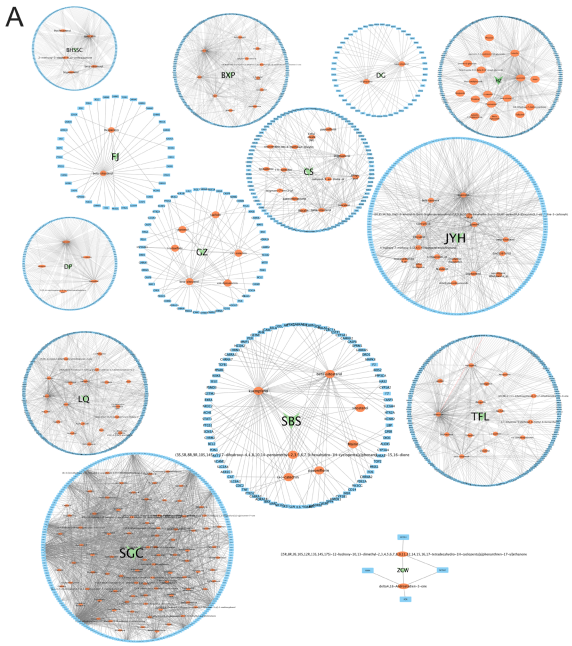

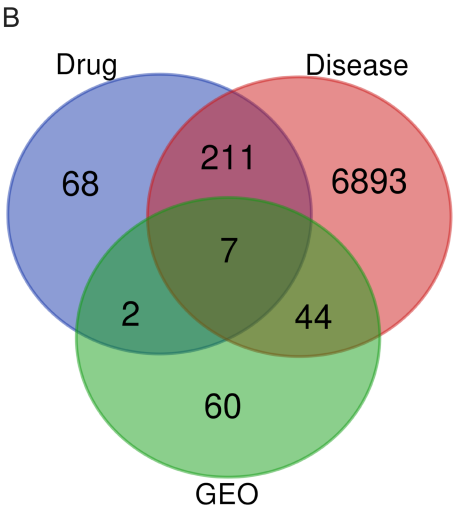

C

Intersection genes in drug composition, disease, and transcriptomics network

Gene Symbol	Description
COL1A1	Collagen alpha-1(I) chain
LDLR	Low-density lipoprotein receptor
VEGFA	Vascular endothelial growth factor A
MYC	Myc proto-oncogene protein
EGFR	Epidermal growth factor receptor
MCL1	Induced myeloid leukemia cell differentiation protein Mcl-1
FOSL2	Fos-related antigen 2

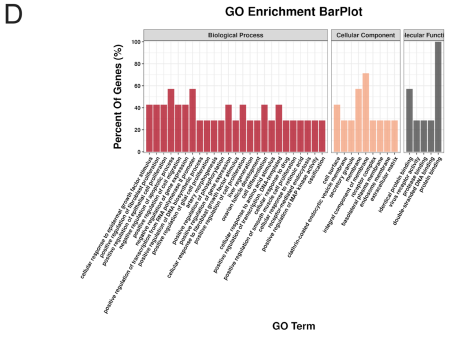

E

Biological processes of intersection gene enrichment (top 10)

Term	Genes
GO:0043066~negative regulation of apoptotic process	MYC, EGFR, MCL1, VEGFA
GO:0045944~positive regulation of transcription from RNA polymerase II promoter	MYC, EGFR, FOSL2, VEGFA
GO:0071364~cellular response to epidermal growth factor stimulus	COL1A1, MYC, EGFR
GO:0048146~positive regulation of fibroblast proliferation	MYC, EGFR, FOSL2
GO:0050679~positive regulation of epithelial cell proliferation	MYC, EGFR, VEGFA
GO:0030335~positive regulation of cell migration	COL1A1, EGFR, VEGFA
GO:0010629~negative regulation of gene expression	MYC, LDLR, VEGFA
GO:0010628~positive regulation of gene expression	MYC, LDLR, VEGFA
GO:0008284~positive regulation of cell proliferation	MYC, EGFR, VEGFA
GO:0030154~cell differentiation	EGFR, MCL1, VEGFA

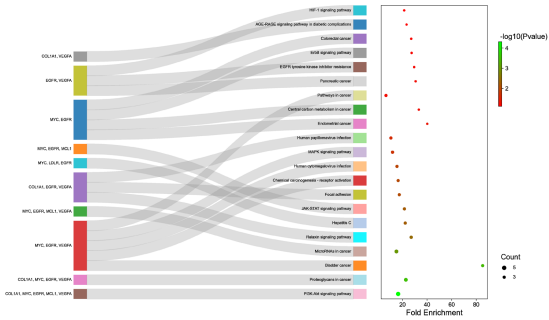

Figure 3. Network pharmacology results. A. Network diagram of drugs - small molecule components - targets (▼: Drugs; ⬭: Small Molecule; ▬: Targets). B. Intersection of drug, disease targets, and transcriptome targets. C. Intersection genes in drug composition, disease, and transcriptomics network. D. GO Enrichment Results of Target Genes. E. Biological processes of intersection gene enrichment (top 10). F. KEGG Enrichment Results of Target Genes. Notes: All TCM decoction pieces in the formula are abbreviated according to the initial letters of their Chinese names,such as Rhizoma Polygoni Cusp (HZ), Lonicera japonica Thunb (JYH), Forsythia suspensa (LQ), Rhizoma smilacis glabrae (TFL), Cortex dictamni (BXP), Radix Stephaniae Tetrandrae (FJ), Paeoniae Radix Alba (SBS), Cassia twig (GZ), Radix glycyrrhizae (SGC), Hedyotis diffusa Willd (BHSSC), Cortex moutan (DP), Radix paeoniae rubrathe (CS), and Angelicae Pubescentis Radix (DG).

ing 10 normal synovial tissues, 10 osteoarthritis synovial tissues, and 13 RA synovial tissue samples. Using the limma analysis package built into GEO2R, differential gene expression analysis was conducted on chip data from 10 normal and 23 abnormal tissues. The screening criteria for significantly differentially expressed genes were set as follows: $P < 0.05$ and $|logFC| > 1.0$. Additionally, the chip from GSE55235 was selected for analysis, involving 30 synovial samples, including 10 normal tissues and 20 samples of RA or osteoarthritis (abnormal tissues). The screening method and criteria for significantly different genes were the same as those described above. After removing duplicates from the intersection genes of the two databases, we obtained 113 disease targets based on transcriptomic data from the GEO database (Supplementary Table 2). After drawing of the Venn diagram to obtain the intersection of drug targets, disease targets, and transcriptome targets, a total of seven targets were found to meet the requirements, including COL1A1 (Collagen alpha-1(I) chain), LDLR (Low-density lipoprotein receptor), VEGFA (Vascular endothelial growth factor A), MYC (Myc proto-oncogene protein), MCL1 (Induced myeloid leukemia cell differentiation protein Mcl-1), EGFR (Epidermal growth factor receptor), and FOSL2 (Fos-related antigen 2). The specific results for the seven targets are shown in **Figure 3B**, **3C**.

The signal pathway enrichment of these seven genes was searched using the DAVID database, and the GO analysis results are shown in (**Figure 3D**). These seven genes were mainly enriched in biological processes (BP), cellular components (CC), and molecular functions (MF). After GO analysis, the main biological processes enriched in target genes included: GO:0043066-negative regulation of apoptotic process; GO:0045944-positive regulation of transcription from RNA polymerase II promoter; GO:0071364-cellular response to epidermal growth factor stimulus; GO:0048146-positive regulation of fibroblast proliferation; and GO:0050679-positive regulation of epithelial cell proliferation; GO:0010629-negative regulation of gene expression (**Figure 3E**). After KEGG pathway enrichment analysis, the main pathway enrichment of target genes included: hsa04151: PI3K-Akt signaling pathway; hsa05205: proteoglycans in cancer; hsa05206: microRNAs in cancer; hsa05219: bladder cancer; hsa04926: relaxin signaling pathway; hsa05160: hepatitis C; hsa04630: JAK-STAT signaling pathway; and hsa04510: focal adhesion (**Figure 3F**).

TCM-compounds-biological functional modules-biomolecular network analysis

The compound Chinese medicine and seven target genes were searched for corresponding binding small molecules using VOOKUP function. The Closeness and Degree parameters were automatically analyzed to construct the target network, as shown in **Figure 4A**. Based on the Degree values, we identified VEGFA, EGFR, and MYC as the key proteins that play a significant role in RA (**Figure 4A**). Based on GO analysis results, the functions of the seven target genes were summarized as drug reactions, transcriptional regulation, cell proliferation, and apoptosis. A network diagram of the traditional Chinese medicine-compound biological function module-biomolecule was constructed to describe the potential biological mechanisms in the formula, as shown in **Figure 4B**. Through KEGG analysis, possible signaling pathways related to RA were predicted (**Figure 4C**). We selected hsa01521, EGFR tyrosine kinase inhibitor resistance; hsa04066, HIF-1 signaling pathway; and hsa04370, VEGF signaling pathway to draw pathway maps (**Figure 4D**).

Molecular docking verification

In this study, molecular docking was conducted for 9 candidate compounds and 7 target proteins. MOL000006 is a flavonoid, which has strong hydrophobicity and can form strong hydrophobic interactions with the amino acids (ILE-1013, ALA-1015, LEU-1012, ALA-766) at the active site of the COL1A1 protein, playing an important role in stabilizing small molecules in the protein cavity (**Figure 5A**). Additionally, it can form strong hydrogen bonds with the amino acids ARG-1019, LEU-1012, ARG-765, and GLN-1010 at the protein site, making a significant contribution to anchoring small molecules within the protein cavity. The MOL000098 compound matched well with the EGFR protein active site, capable of forming various interactions with amino acids, such as hydrogen bonding interactions (LYS-721, GLN-767, and LEU-768) and hydrophobic interactions (VAL-702, LEU-768, LEU-820, LEU-753, MET-742, and MET-769) (**Figure 5B**). These interactions can

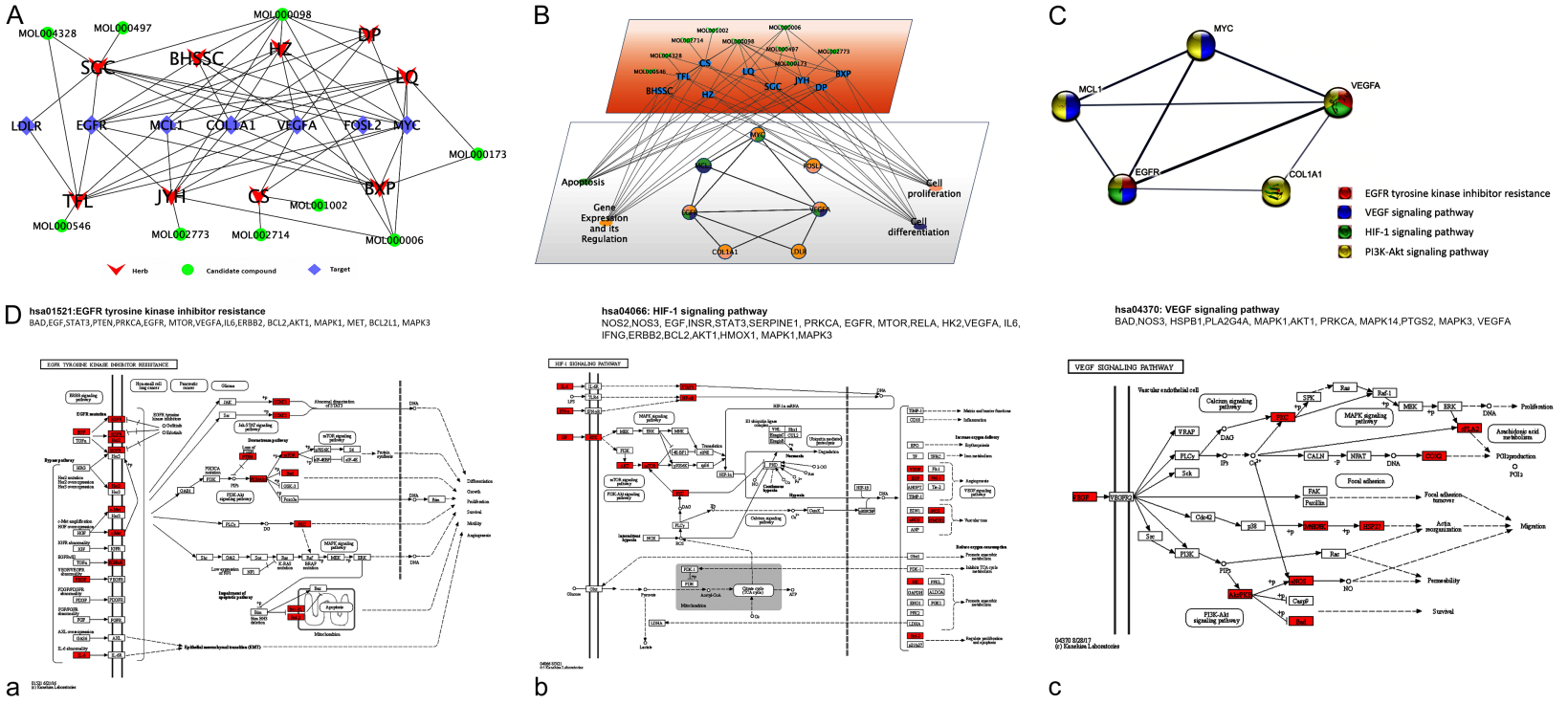

Figure 4. Biomolecular network results of TCM, compounds, and biological functional modules. A. Compound-target network between 9 candidate compounds and 7 targets in the formula of QYCD. B. Potential biological mechanisms of QYCD described by a biomolecular network based on TCM, compound, and biological functional module. C. Key gene networks and rheumatoid arthritis related signaling pathways in the prescription target network. D. Typical signaling pathway diagrams: (a) EGFR; (b) HIF-1; (c) VEGF. Key gene networks and rheumatoid arthritis related signaling pathways in the prescription target network. Notes: All TCM decoction pieces in the formula are abbreviated according to the initial letters of their Chinese names,such as Rhizoma Polygoni Cusp (HZ), Lonicera japonica Thunb (JYH), Forsythia suspensa (LQ), Rhizoma smilacis glabrae (TFL), Cortex dictamni (BXP), Radix glycyrrhizae (SGC), Hedyotis diffusa Willd (BHSSC), Cortex moutan (DP), Radix paeoniae rubrathe (CS).

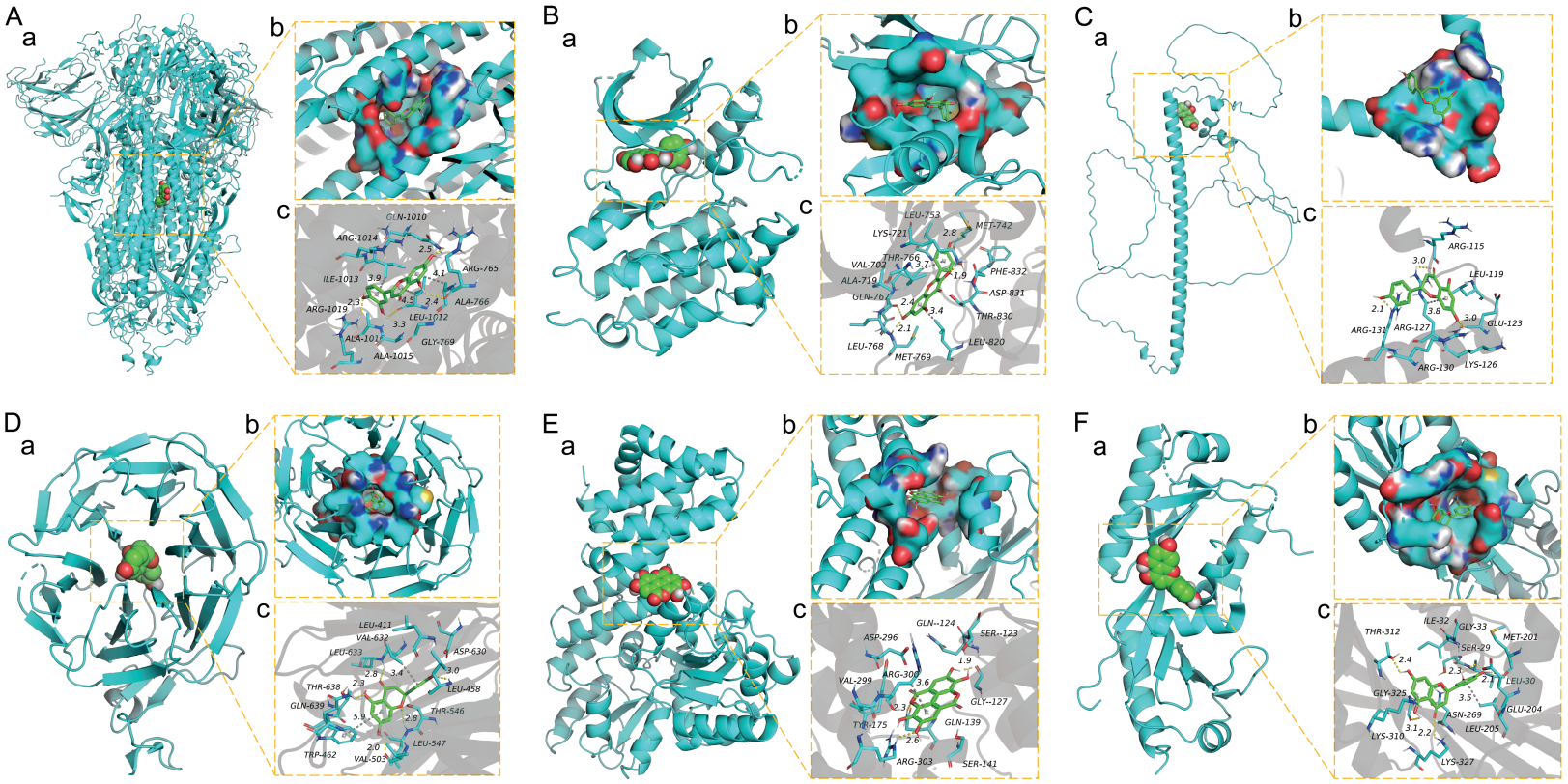

H

Name	COL1A1	EGFR	FOSL2	LDLR	MCL1	MYC	VEGFA
MOL000006	-8.49	-9.03	-5.66	-7.21	-7.67	-7.81	-7.14
MOL000098	-7.63	-9.20	-5.14	-7.22	-7.82	-6.89	-7.31
MOL000173	-7.86	-8.12	-5.49	-7.44	-7.35	-7.26	-6.55
MOL000497	-7.60	-8.43	-5.56	-8.06	-7.90	-6.59	-6.59
MOL000546	-8.08	-8.72	-5.12	-7.38	-6.75	-6.11	-6.52
MOL001002	-8.03	-9.00	-5.61	-7.50	-8.17	-7.45	-6.95
MOL002714	-8.15	-8.53	-5.25	-7.54	-7.54	-7.50	-7.36
MOL002773	-6.39	-6.86	-4.86	-5.36	-6.48	-6.23	-5.90
MOL004328	-8.14	-6.92	-5.73	-8.43	-7.05	-6.75	-7.19

Figure 5. The binding mode of nine compounds with seven target proteins individually. A is the 3D structure of complex, B shows the pocket surface of protein, C is the 3D binding mode of complex. Yellow and gray dash represent the hydrogen bond interaction or pi-stacking. (A) COL1A1-MOL000006. (B) EGFR-MOL000098. (C) FOSL2-MOL004328. (D) LDLR - MOL004328. (E) MCL1 - MOL001002. (F) MYC-MOL000006. (G) VEGFA-MOL002714. (H) Molecular docking results.

effectively promote the formation of stable complexes between the small molecules and proteins. MOL004328 binds weakly to the FOSL2 target, but can form strong hydrogen bonding interactions with amino acids (ARG-131, ARG-130, and ARG-127) at the protein site, playing a crucial role in stabilizing the small molecules in the protein pocket (**Figure 5C**). Additionally, this compound can also form hydrophobic interactions with amino acids, such as LEU-119 and ARG-127, which greatly aids in stabilizing small molecules. MOL004328 compounds matched well with LDLR protein sites, capable of forming hydrogen bonds (LEU-633, VAL-503, LEU-547, and LEU-458) and hydrophobic (TRP-462, VAL-503, VAL-632, LEU-411, and LEU-458) interactions (**Figure 5D**). These interactions effectively promote the formation of stable complexes between MOL-004328 and PTGS2 proteins.

MOL001002 matches well with the MCL1 target and can form strong hydrogen bonding interactions with the amino acids (GLY-127, ARG-303, GLN-139) of the protein site (**Figure 5E**). In addition, the compound can also form hydrophobic interactions with amino acids, such as VAL-299 and ARG-300, which play an important role in stabilizing small molecules in the protein pocket. MOL000006 exhibited good matching with the MYC target, capable of forming strong hydrogen bonding interactions with amino acids (THR-312, GLY-325, LYS-327, SER-29, and MET-201) at protein sites, playing a crucial role in stabilizing small molecules within the protein pocket (**Figure 5F**). Additionally, this compound can also form hydrophobic interactions with amino acids, such as LEU-205, LEU-30, MET-201, and ILE-32, providing significant assistance in stabilizing small molecules. The MOL002714 compound matches well with VEGFA protein sites, capable of forming hydrogen bonds (THR-319, ASP-323) and π-π conjugation (TYR-365, TRP-304, TYR-299) interactions (**Figure 5G**), effectively promoting the formation of a stable complex between MOL002714 and the PTGS2 protein. In summary, these compounds are capable of forming various interactions, such as hydrogen bonding and hydrophobic interactions with proteins (binding energy less than -6 kcal/mol), enabling them to form stable complexes with proteins and making them potentially active compounds. The molecular docking results are presented in **Figure 5H**.

Discussion

Due to the complexity of RA, its specific etiology and pathogenesis are not yet fully understood. Genetic susceptibility, environmental factors that trigger pathogenic autoimmune inflammatory responses against synovial and cartilage components, as well as immune inflammatory cell infiltration that induces synovial cell proliferation and transformation into autonomously proliferating cells, and the dysregulation of inflammatory cell cytokine production are the main factors leading to RA [15-17]. Autoantigens are presented by antigen-presenting cells (APCs) to CD4+ T cells, thereby initiating specific immune responses. At the same time, activated T cells, macrophages, and other immune cells migrate to the synovium. These immune cells regulate each other, forming a complex network that participates in the onset and development of RA. Migrating immune cells are activated, differentiated, and acquire mature phenotypes in the joints; they secrete various inflammatory cytokines and matrix metalloproteinases; and they participate in multiple processes of RA, including synovial inflammation, synovial proliferation, angiogenesis, cartilage degradation, and bone destruction, ultimately leading to joint deformities and loss of function [18]. The imbalance between pro-inflammatory and anti-inflammatory cytokines leads to a systemic inflammatory state in patients with RA and plays a crucial role in inflammation, joint destruction, and RA-related diseases. The cytokine-mediated inflammatory process plays an important role in the progression of RA, and this inflammatory process can induce metabolic changes [19]. Metabolites affect the development of the immune system through mechanisms involving antigen receptors, co-stimulatory molecules, growth factors, hormones, cytokines, environmental factors, and other regulatory signals.

A total of 205 active ingredients were screened from QYCD, including flavonoids, quinones, phenols, phenylpropanoids, and alkaloids. Among them, the core active substances include baicalin, ellagic acid, luteolin, quercetin, β-carotene, hanbaicalin, licorice flavonoid A, diosgenin, and naringenin, corresponding to 294 identified targets, of which 196 target components overlap with RA disease targets. These overlapping targets are potential therapeutic targets for QYCD treatment. By comparing the

targets of QYCD and RA, COL1A1, LDLR, VEGFA, MYC, EGFR, MCL1, and FOSL2 were found to be key target genes for QYCD treatment of RA, involving important biological pathways such as DNA transcription regulation, RNA polymerase II promoter transcription regulation, gene expression regulation, and signal transduction. COL1A1 is a type I collagen that accounts for more than 80% of bone tissue. It is mainly synthesized by osteoblasts and is a major component of the bone matrix. It can promote collagen maturation and osteoblast differentiation, and facilitate mineral salt deposition, thereby accelerating the formation of bone tissue. MCL1 is a member of the BCL-2 gene family, located in the endoplasmic reticulum, particularly at the mitochondrial membrane [20], and is an important factor regulating cell differentiation and anti-apoptosis [21]. The imbalance between pro-apoptotic and anti-apoptotic genes caused by abnormal expression of apoptosis-related genes is one of the important reasons for the inhibition of apoptosis in RA-FLS (Fibroblast-like synoviocytes) [22]. MCL1 is highly expressed in RA-FLS, inhibiting the pro-apoptotic effects of Bim, Bax, and Bak [23]. MCL1 is closely related to the survival and apoptosis of immune cells such as T and B lymphocytes and macrophages [24]. The expression of MCL1 is regulated by the JAK/STAT and mitogen-activated protein kinase (MAPK) signaling pathways in the nucleus, as well as the PI3K/AKT signaling pathway in the cytoplasm. The JAK-STAT signaling pathway is an important cytokine signaling pathway involved in the pathophysiological processes of RA [25] and plays a significant role in the body's inflammatory response.

EGFR belongs to the tyrosine kinase receptor superfamily and is a transmembrane protein that transmits signals from the extracellular environment to the intracellular space. After EGFR binds with ligands such as epidermal growth factor and transforming growth factor-alpha (TGF-α), it induces the PI3K/AKT signaling pathway, stimulating the expression of cytokines such as VEGF, IL-6, IL-8, MCP-1, and MMP-3, and participates in various cellular processes including migration, proliferation, differentiation, and apoptosis [26]. High expression of EGFR has been observed in the serum, synovium [27], and sub-synovial tissues of RA patients, suggesting the potential value of EGFR as a new therapeutic target for RA [28]. Activated T cells have a high dependence on glucose uptake and utilization, which is crucial for their transformation into effector cells [29]. T cells can still utilize cellular fermentation to generate energy to support mitochondrial oxidative phosphorylation even under aerobic conditions [30], a phenomenon known as the Warburg effect [31]. The PI3K/Akt pathway mainly relies on the expression of mTORC1 and Myc to promote glycolysis and inhibit the oxidative phosphorylation (OXPHOS) process [32]. c-Myc activation promotes glucose uptake and breakdown, regulating the body's glucose metabolism process and the expression of HIF-1α (Hypoxia-inducible factor-1α). HIF-1α is a transcriptionally active nuclear protein that plays a regulatory role in hypoxic adaptation, inflammation processes, and tumor growth, and is expressed in innate immune cells such as macrophages, dendritic cells, neutrophils, and Th17 cells [33]. In these cells, HIF-1α plays an important role in pathological stress and environmental adaptation responses. Immune cells generate different energy demands based on their activation state and adaptively change their energy metabolism patterns. The HIF pathway provides these cells with a metabolic energy conversion model, enabling them to respond adaptively to changing energy demands and adapt to the hypoxic conditions commonly present in inflamed tissues. Research has found that hypoxia and inflammation regions overlap in RA joints, with a large number of synovial cells, lymphocytes, and macrophages infiltrating [34]. Some studies also suggest that Myc and HIF-1α may become potential targets for RA treatment [35, 36]. KEGG pathway enrihment analysis of 196 target genes mainly involves IL-17 signaling, EGFR signaling, TNF signaling, HIF-1 signaling pathways, and Th17 cell differentiation pathways, which are closely related to inflammatory response and bone metabolism. The above results indicate that QYCD exerts an overall regulatory effect on the body through multiple components and multiple targets in various ways.

This study preliminarily explored the mechanisms of Qingre Yangyin Chushi Decoction (QYCD) in treating rheumatoid arthritis through network pharmacology, successfully screening core components, core targets, and key biological pathways. Due to technical and conditional

limitations, there are still shortcomings in this study. These include, not conducting in-depth research on the therapeutic effects and mechanisms of the screened candidate compounds; no cellular level research was conducted, such as using blocking drugs or agonists to screen key signaling pathways, overexpressing or inhibiting the expression of certain molecules, in order to more accurately identify QYCD targets and provide new strategies for the treatment of RA. Further molecular level research on this topic will continue in the future.

Conclusion

QYCD alleviates arthritis inflammation and bone damage in collagen-induced arthritic rats, possibly by regulating inflammatory cytokines and the body's immunity, restoring the chronic inflammation state to normal homeostasis. Network pharmacology analysis identifies key target genes COL1A1, LDLR, VEGFA, MYC, EGFR, MCL1, and FOSL2, which are involved in crucial biological pathways such as DNA transcription regulation and signal transduction, while nine candidate compounds screened in this study show potential as active agents for rheumatoid arthritis treatment. The treatment of RA with QYCD exerts its effects through a multi-target and multi-pathway approach, supporting our previous experimental results, while stronger supporting evidence awaits further investigation.

Acknowledgements

We express our gratitude to all those who assisted us in this study. We acknowledge the invaluable contributions of numerous researchers, yet due to space limitations, we are unable to cite their published articles. This work was supported by the Science and Technology Development Fund of the TCM Science Research Project Fund of Hebei Provincial Administration of TCM (grant no. B2025057), the Beijing Hospital of TCM, Capital Medical University (grant no. LYYB202222) and Natural Science Foundation of Beijing Municipality (grant no. 7172101).

Disclosure of conflict of interest

None.

Abbreviations

AI, arthritis index; AKT, serine /threonine protein kinase; BCL-2, B-cell lymphoma-2; CII, bovine type II collagen; CIA, collagen-induced arthritis; COL1A1, collagen alpha-1(I) chain; MYC, myelocytomatosis oncogene; DAVID, the database for annotation, visualization and integrated discovery; DMARDs, disease-modifying antirheumatic drugs; EGFR, epidermal growth factor receptor; ELISA, enzyme-linked immunosorbent assay; FOSL2, fos-related antigen 2; GEO, gene expression omnibus database; GO, gene ontology; HE, hematoxylin-eosin; HIF, hypoxia inducible factor; IFA, incomplete Freund's adjuvant; IFN-γ, interferon-γ; IL, interleukin; JAK, janus kinase; KEGG, kyoto encyclopedia of genes and genomes; LDLR, low-density lipoprotein receptor; MAPK, mitogen-activated protein kinase; MCL1, Induced myeloid leukemia cell differentiation protein Mcl-1; MMP, matrixmetalloproteinases; MTX, methotrexate; NCBI, national center of biotechnology information; QYCD, qingre yangyin chushi decode; RA, rheumatoid arthritis; RANKL, receptor activator for nuclear factor-κB ligand; RA-SM, rheumatoid arthritis synovial membrane; STAT, signal transducer and activator of transcription; TCM, traditional Chinese medicine; TCMSP, traditional Chinese medicine systems pharmacology; TGF, transforming growth factor; Th cell, helper T cell; TNF-α, tumor necrosis factor-α; TRAP, tartrate resistant acid phosphatase; VEGFA, Vascular endothelial growth factor A.

Address correspondence to: Mi-Feng Liu, Beijing Hospital of Traditional Chinese Medicine, Capital Medical University, No. 23 Meishuguan Back Street, Dongcheng District, Beijing 100010, China. E-mail: liumifeng@bjzhongyi.com

References

[1] Lazzerini PE, Capecchi PL and Laghi-Pasini F. Systemic inflammation and arrhythmic risk: lessons from rheumatoid arthritis. Eur Heart J 2017; 38: 1717-1727.

[2] Wang D, Zhang J, Lau J, Wang S, Taneja V, Matteson EL and Vassallo R. Mechanisms of lung disease development in rheumatoid arthritis. Nat Rev Rheumatol 2019; 10: 581-596.

[3] Figus FA, Piga M, Azzolin I, McConnell R and Iagnocco A. Rheumatoid arthritis: extra-articular manifestations and comorbidities. Autoimmun Rev 2021; 20: 102776.

[4] Scott DL, Wolfe F and Huizinga TW. Rheumatoid arthritis. Lancet 2010; 376: 1094-1108.
[5] Catrina AI, Deane KD and Scher JU. Gene, environment, microbiome and mucosal immune tolerance in rheumatoid arthritis. Rheumatol (Oxford) 2016; 55: 391-402.
[6] Mueller A, Payandeh Z, Mohammadkhani N, Mubarak SMH, Zakeri A, Alagheband Bahrami A, Brockmueller A and Shakibaei M. Recent advances in understanding the pathogenesis of rheumatoid arthritis: new treatment strategies. Cells 2021; 10: 3017.
[7] Singh JA, Saag KG, Bridges SL, Akl EA, Bannuru RR, Sullivan MC, Vaysbrot E, McNaughton C, Osani M, Shmerling RH, Curtis JR, Furst DE, Parks D, Kavanaugh A, O'Dell J, King C, Leong A, Matteson EL, Schousboe JT, Drevlow B, Ginsberg S, Grober J, St Clair EW, Tindall E, Miller AS and McAlindon T. 2015 American College of Rheumatology Guideline for the Treatment of Rheumatoid Arthritis. Arthrit Care Res (Hoboken) 2016; 68: 1-25.
[8] Smolen JS, Landewé R, Bijlsma J, Burmester G, Chatzidionysiou K, Dougados M, Nam J, Ramiro S, Voshaar M, van Vollenhoven R, Aletaha D, Aringer M, Boers M, Buckley CD, Buttgereit F, Bykerk V, Cardiel M, Combe B, Cutolo M, van Eijk-Hustings Y, Emery P, Finckh A, Gabay C, Gomez-Reino J, Gossec L, Gottenberg J, Hazes JMW, Huizinga T, Jani M, Karateev D, Kouloumas M, Kvien T, Li Z, Mariette X, McInnes I, Mysler E, Nash P, Pavelka K, Poór G, Richez C, van Riel P, Rubbert-Roth A, Saag K, Da Silva J, Stamm T, Takeuchi T, Westhovens R, de Wit M and van der Heijde D. EULAR recommendations for the management of rheumatoid arthritis with synthetic and biological disease-modifying antirheumatic drugs: 2016 update. Ann Rheum Dis 2017; 76: 960-977.
[9] Bécède M, Alasti F, Gessl I, Haupt L, Kerschbaumer A, Landesmann U, Loiskandl M, Supp GM, Smolen JS and Aletaha D. Risk profiling for a refractory course of rheumatoid arthritis. Semin Arthritis Rheu 2019; 49: 211-217.
[10] Sepriano A, Kerschbaumer A, Smolen JS, van der Heijde D, Dougados M, van Vollenhoven R, McInnes IB, Bijlsma JW, Burmester GR, de Wit M, Falzon L and Landewé R. Safety of synthetic and biological DMARDs: a systematic literature review informing the 2019 update of the EULAR recommendations for the management of rheumatoid arthritis. Ann Rheum Dis 2020; 79: 760-770.
[11] Yang K, Zeng L, Long Z, He Q, Xiang W, Ge A, Zhen H, Xiao W and Ge J. Efficacy and safety of total glucosides of paeony in the treatment of 5 types of inflammatory arthritis: A systematic review and meta-analysis. Pharmacol Res 2023; 195: 106842.
[12] Qu P, Wang H, Wang W, Du S, Peng Z, Hu Q and Tang X. Efficacy and safety of Duhuo-Jisheng decoction in rheumatoid arthritis: a systematic review and meta-analysis of 42 randomized controlled trials. Medicine (Baltimore) 2023; 102: e35513.
[13] Brand DD, Latham KA and Rosloniec EF. Collagen-induced arthritis. Nat Protoc 2007; 2: 1269-1275.
[14] Hayer S, Vervoordeldonk MJ, Denis MC, Armaka M, Hoffmann M, Bäcklund J, Nandakumar KS, Niederreiter B, Geka C, Fischer A, Woodworth N, Blüml S, Kollias G, Holmdahl R, Apparailly F and Koenders MI. 'SMASH' recommendations for standardised microscopic arthritis scoring of histological sections from inflammatory arthritis animal models. Ann Rheum Dis 2021; 80: 714-726.
[15] Iebba F, Di Sora F, Tarasi A, Leti W and Montella F. Rheumatoid arthritis: a typical multifactorial genetic disease: review of the literature. Recenti Prog Med 2011; 4: 175-182.
[16] Venetsanopoulou AI, Alamanos Y, Voulgari PV and Drosos AA. Epidemiology and risk factors for rheumatoid arthritis development. Mediterr J Rheumatol 2023; 4: 404-413.
[17] Lamba A and Taneja V. Gut microbiota as a sensor of autoimmune response and treatment for rheumatoid arthritis. Immunol Rev 2024; 1: 90-106.
[18] McInnes IB and Schett G. The pathogenesis of rheumatoid arthritis. New Engl J Med 2011; 365: 2205-2219.
[19] Cederholm T, Wretlind B, Hellström K, Andersson B, Engström L, Brismar K, Scheynius A, Forslid J and Palmblad J. Enhanced generation of interleukins 1 beta and 6 may contribute to the cachexia of chronic disease. Am J Clin Nutr 1997; 65: 876-882.
[20] Gan P, Wu H, Zhu Y, Shu Y and Wei Y. Glycolysis, a driving force of rheumatoid arthritis. Int Immunopharmacol 2024; 132: 111913.
[21] Varadarajan S, Butterworth M, Wei J, Pellecchia M, Dinsdale D and Cohen GM. Sabutoclax (BI97C1) and BI112D1, putative inhibitors of MCL-1, induce mitochondrial fragmentation either upstream of or independent of apoptosis. Neoplasia 2013; 5: 568-578.
[22] Bartok B and Firestein GS. Fibroblast-like synoviocytes: key effector cells in rheumatoid arthritis. Immunol Rev 2010; 233: 233-255.
[23] Liu H, Eksarko P, Temkin V, Haines GK, Perlman H, Koch AE, Thimmapaya B and Pope RM. Mcl-1 is essential for the survival of synovial fibroblasts in rheumatoid arthritis. J Immunol 2005; 175: 8337-8345.
[24] Yang-Yen HF. Mcl-1: a highly regulated cell death and survival controller. J Biomed Sci 2006; 13: 201-204.

[25] George G, Shyni GL and Raghu KG. Current and novel therapeutic targets in the treatment of rheumatoid arthritis. Inflammopharmacology 2020; 28: 1457-1476.
[26] Spel L and Martinon F. Inflammasomes contributing to inflammation in arthritis. Immunol Rev 2020; 294: 48-62.
[27] Chen SY, Shiau AL, Wu CL and Wang CR. Amelioration of experimental arthritis by intra-articular injection of an epidermal growth factor receptor tyrosine kinase inhibitor. Clin Exp Rheumatol 2025; 33: 839-843.
[28] Li Z, Xu M, Li R, Zhu Z, Liu Y, Du Z, Zhang G and Song Y. Identification of biomarkers associated with synovitis in rheumatoid arthritis by bioinformatics analyses. Biosci Rep 2020; 40: BSR20201713.
[29] Liu Y, Wang F, Peng D, Zhang D, Liu L, Wei J, Yuan J, Zhao L, Jiang H, Zhang T, Li Y, Zhao C, He S, Wu J, Yan Y, Zhang P, Guo C, Zhang J, Li X, Gao H and Li K. Activation and antitumor immunity of CD8+ T cells are supported by the glucose transporter GLUT10 and disrupted by lactic acid. Sci Transl Med 2024; 762: eadk7399.
[30] Fernández-Ramos AA, Poindessous V, Marchetti-Laurent C, Pallet N and Loriot MA. The effect of immunosuppressive molecules on T-cell metabolic reprogramming. Biochimie 2016; 127: 23-36.
[31] Koppenol WH, Bounds PL and Dang CV. Otto Warburg's contributions to current concepts of cancer metabolism. Nat Rev Cancer 2011; 11: 325-337.
[32] Fontana F, Giannitti G, Marchesi S and Limonta P. The PI3K/Akt pathway and glucose metabolism: a dangerous liaison in cancer. Int J Biol Sci 2024; 8: 3113-3125.
[33] Dang EV, Barbi J, Yang HY, Jinasena D, Yu H, Zheng Y, Bordman Z, Fu J, Kim Y, Yen HR, Luo W, Zeller K, Shimoda L, Topalian SL, Semenza GL, Dang CV, Pardoll DM and Pan F. Control of T(H)17/T(reg) balance by hypoxia-inducible factor 1. Cell 2011; 5: 772-784.
[34] Li M, Song C and Dai M. The role of HIF signal mediated autophagy dysfunction in synovial fibroblasts in rheumatoid arthritis and the targeted regulation of kaempferol. Tissue Cell 2025; 98: 103172.
[35] Zhang YF, Zhang ZH, Li M, Wang JY, Xing Y, Ri M, Jin CH, Xu GH, Piao LX, Zuo HX, Jin HL, Ma J and Jin X. Britannin stabilizes T cell activity and inhibits proliferation and angiogenesis by targeting PD-L1 via abrogation of the crosstalk between Myc and HIF-1α in cancer. Phytomedicine 2021; 81: 153425.
[36] Meng B, Liu FY, Liu MM, Yu LC, Zhang WT, Zhou MY, Liu SY, Li R and Cai L. AMSP-30 m as a novel HIF-1α inhibitor attenuates the development and severity of adjuvant-induced arthritis in rats: Impacts on synovial apoptosis, synovial angiogenesis and sonic hedgehog signaling pathway. Int Immunopharmacol 2022; 103: 108467.

Supplementary Table 1. Basic information of the main active ingredients in QYCD

No.	MOL_ID	molecule_name	OB%	MW	DL	Source
1	MOL001663	(4aS,6aR,6aS,6bR,8aR,10R,12aR,14bS)-10-hydroxy-2,2,6a,6b,9,9,12a-heptamethyl-1,3,4,5,6,6a,7,8,8a,10,11,12,13,14b-tetradecahydropicene-4a-carboxylic acid	32.02801	456.78	0.75713	Hedyotis diffusa Willd
2	MOL001646	2,3-dimethoxy-6-methyanthraquinone	34.8586	282.31	0.26255	Hedyotis diffusa Willd
3	MOL001670	2-methoxy-3-methyl-9,10-anthraquinone	37.82771	252.28	0.20517	Hedyotis diffusa Willd
4	MOL001659	Poriferasterol	43.82985	412.77	0.75596	Hedyotis diffusa Willd
5	MOL006244	(1R,4R,6S,8aR)-1-(3-furyl)-4,6-dihydroxy-5,8a-dimethyl-4,6,7,8-tetrahydro-1H-isochromen-3-one	49.09192	278.33	0.19406	Cortex dictamni
6	MOL006233	3'-O-methyl taxifolin	48.35707	318.3	0.30399	Cortex dictamni
7	MOL006262	7alpha-acetylobacunol	36.0753	498.62	0.7081	Cortex dictamni
8	MOL006272	9alpha-hydroxyfraxinellone-9-o-beta-d-glucoside	55.52135	424.49	0.6208	Cortex dictamni
9	MOL006235	Dasycarpamin	59.13574	303.39	0.21247	Cortex dictamni
10	MOL006257	dictamnusine_qt	69.27396	278.33	0.19398	Cortex dictamni
11	MOL006261	Isomaculosidine	31.99411	259.28	0.19599	Cortex dictamni
12	MOL006236	Limonin diosphenol	91.68747	484.54	0.54898	Cortex dictamni
13	MOL013352	Obacunone	43.28625	454.56	0.76724	Cortex dictamni
14	MOL006268	preskimmianine	42.14344	303.39	0.21315	Cortex dictamni
15	MOL002663	Skimmianin	40.13655	259.28	0.19638	Cortex dictamni
16	MOL006270	tirucallane	44.01594	426.8	0.74915	Cortex dictamni
17	MOL006271	trichirubine,b	35.50504	560.74	0.27108	Cortex dictamni
18	MOL005043	campest-5-en-3beta-ol	37.57682	400.76	0.71481	Cortex dictamni, Radix paeoniae rubrathe
19	MOL006990	(1S,2S,4R)-trans-2-hydroxy-1,8-cineole-B-D-glucopyranoside	30.25241	332.44	0.27464	Radix paeoniae rubrathe
20	MOL006992	(2R,3R)-4-methoxyl-distylin	59.98325	318.3	0.29949	Radix paeoniae rubrathe
21	MOL006994	1-o-beta-d-glucopyranosyl-8-o-benzoylpaeonisuffrone_qt	36.01306	302.35	0.29897	Radix paeoniae rubrathe
22	MOL006996	1-o-beta-d-glucopyranosylpaeonisuffrone_qt	65.08187	332.38	0.35391	Radix paeoniae rubrathe
23	MOL007008	4-ethyl-paeoniflorin_qt	56.86958	332.38	0.44483	Radix paeoniae rubrathe
24	MOL007012	4-o-methyl-paeoniflorin_qt	56.70352	332.38	0.42562	Radix paeoniae rubrathe
25	MOL007014	8-debenzoylpaeonidanin	31.74315	390.43	0.45389	Radix paeoniae rubrathe
26	MOL007018	9-ethyl-neo-paeoniaflorin A_qt	64.41989	334.4	0.29598	Radix paeoniae rubrathe
27	MOL007004	Albiflorin	30.24614	480.51	0.77038	Radix paeoniae rubrathe
28	MOL007005	albiflorin_qt	48.70012	318.35	0.32628	Radix paeoniae rubrathe
29	MOL002714	Baicalein	33.51892	270.25	0.20888	Radix paeoniae rubrathe
30	MOL002776	Baicalin	40.12361	446.39	0.75264	Radix paeoniae rubrathe
31	MOL001002	ellagic acid	43.06456	302.2	0.43417	Radix paeoniae rubrathe
32	MOL002883	Ethyl oleate (NF)	32.39739	310.58	0.19061	Radix paeoniae rubrathe
33	MOL007022	evofolinB	64.73662	318.35	0.22232	Radix paeoniae rubrathe
34	MOL007025	isobenzoylpaeoniflorin	31.13867	584.62	0.54234	Radix paeoniae rubrathe
35	MOL007016	Paeoniflorigenone	65.33411	318.35	0.36711	Radix paeoniae rubrathe
36	MOL004355	Spinasterol	42.97937	412.77	0.75534	Radix paeoniae rubrathe
37	MOL006999	stigmast-7-en-3-ol	37.42312	414.79	0.75088	Radix paeoniae rubrathe
38	MOL007369	4-O-methylpaeoniflorin_qt	67.23726	332.38	0.42561	Cortex moutan
39	MOL007374	5-[[5-(4-methoxyphenyl)-2-furyl] methylene] barbituric acid	43.44402	312.3	0.30018	Cortex moutan
40	MOL007382	mudanpioside-h_qt 2	42.35942	336.37	0.37019	Cortex moutan
41	MOL007384	paeonidanin_qt	65.31306	330.41	0.3495	Cortex moutan
42	MOL007003	benzoyl paeoniflorin	31.13867	584.62	0.54227	Cortex moutan, Radix paeoniae rubrathe

43	MOL002341	Hesperetin	70.31209	302.3	0.27252	Radix Stephaniae Tetrandrae
44	MOL002333	Tetraneurin A	35.39892	322.39	0.30933	Radix Stephaniae Tetrandrae
45	MOL000073	ent-Epicatechin	48.95984	290.29	0.24162	Cassia twig
46	MOL011169	Peroxyergosterol	44.39152	428.72	0.82	Cassia twig
47	MOL013281	6,8-Dihydroxy-7-methoxyxanthone	35.82614	258.24	0.21218	Rhizoma Polygoni Cusp
48	MOL002259	Physciondiglucoside	41.64856	608.6	0.63145	Rhizoma Polygoni Cusp
49	MOL013287	Physovenine	106.2136	262.34	0.18963	Rhizoma Polygoni Cusp
50	MOL013288	Picralinal	58.00695	366.45	0.7541	Rhizoma Polygoni Cusp
51	MOL002268	rhein	47.06521	284.23	0.27678	Rhizoma Polygoni Cusp
52	MOL002280	Torachrysone-8-O-beta-D-(6'-oxayl)-glucoside	43.01996	480.46	0.73687	Rhizoma Polygoni Cusp
53	MOL000492	(+)-catechin	54.82643	290.29	0.24164	Rhizoma Polygoni Cusp, Cortex moutan, Paeoniae Radix Alba, Radix paeoniae rubrathe, Cassia twig
54	MOL000006	Luteolin	36.16263	286.25	0.24552	Rhizoma Polygoni Cusp, Lonicera japonica Thunb, Forsythia suspensa, Cortex dictamni
55	MOL000358	beta-sitosterol	36.91391	414.79	0.75123	Rhizoma Polygoni Cusp, Lonicera japonica Thunb, Forsythia suspensa, Rhizoma smilacis glabrae, Cortex dictamni, Radix Stephaniae Tetrandrae, Paeoniae Radix Alba, Cassia twig, Hedyotis diffusa Willd, Radix paeoniae rubrathe, Angelicae Pubescentis Radix
56	MOL000098	quercetin	46.43335	302.25	0.27525	Rhizoma Polygoni Cusp, Lonicera japonica Thunb, Forsythia suspensa, Rhizoma smilacis glabrae, Cortex dictamni, Radix glycyrrhizae, Hedyotis diffusa Willd, Cortex moutan
57	MOL003006	(-)-(3R,8S,9R,9aS,10aS)-9-ethenyl-8-(beta-D-glucopyranosyloxy)-2,3,9,9a,10,10a-hexahydro-5-oxo-5H,8H-pyrano[4,3-d]oxazolo[3,2-a]pyridine-3-carboxylic acid_qt	87.47219	281.29	0.23288	Lonicera japonica Thunb
58	MOL003062	4,5'-Retro-.beta.,.beta.-Carotene-3,3'-dione, 4',5'-didehydro-	31.22482	562.9	0.55114	Lonicera japonica Thunb
59	MOL003095	5-hydroxy-7-methoxy-2-(3,4,5-trimethoxyphenyl)chromone	51.95651	358.37	0.40656	Lonicera japonica Thunb
60	MOL003101	7-epi-Vogeloside	46.13388	432.47	0.57873	Lonicera japonica Thunb
61	MOL002773	beta-carotene	37.18433	536.96	0.58358	Lonicera japonica Thunb
62	MOL003108	Caeruloside C	55.63653	550.57	0.72896	Lonicera japonica Thunb
63	MOL003111	Centauroside_qt	55.79047	434.48	0.50482	Lonicera japonica Thunb
64	MOL003044	Chryseriol	35.85089	300.28	0.27415	Lonicera japonica Thunb
65	MOL003128	dinethylsecologanoside	48.46185	434.44	0.47786	Lonicera japonica Thunb
66	MOL002914	Eriodyctiol (flavanone)	41.35043	288.27	0.2436	Lonicera japonica Thunb
67	MOL001495	Ethyl linolenate	46.10096	306.54	0.19716	Lonicera japonica Thunb
68	MOL003117	Ioniceracetalides B_qt	61.18571	314.37	0.1927	Lonicera japonica Thunb
69	MOL003059	kryptoxanthin	47.24763	552.96	0.56922	Lonicera japonica Thunb
70	MOL001494	Mandenol	41.9962	308.56	0.19321	Lonicera japonica Thunb
71	MOL002707	phytofluene	43.18173	543.02	0.50316	Lonicera japonica Thunb

72	MOL003014	secologanic dibutylacetal_qt	53.64633	384.57	0.28548	Lonicera japonica Thunb
73	MOL003124	XYLOSTOSIDINE	43.17178	415.51	0.6369	Lonicera japonica Thunb
74	MOL003036	ZINC03978781	43.82985	412.77	0.75647	Lonicera japonica Thunb
75	MOL000422	kaempferol	41.88225	286.25	0.24066	Lonicera japonica Thunb, Forsythia suspensa, Paeoniae Radix Alba, Cortex moutan, Radix glycyrrhizae
76	MOL000449	Stigmasterol	43.82985	412.77	0.75665	Lonicera japonica Thunb, Rhizoma smilacis glabrae, Hedyotis diffusa Willd, Radix paeoniae rubrathe, Angelicae Pubescentis Radix
77	MOL003330	(-)-Phillygenin	95.03641	372.45	0.56703	Forsythia suspensa
78	MOL003295	(+)-pinoresinol monomethyl ether	53.08233	372.45	0.56703	Forsythia suspensa
79	MOL003308	(+)-pinoresinol monomethyl ether-4-D-beta-glucoside_qt	61.20403	372.45	0.56711	Forsythia suspensa
80	MOL003283	(2R,3R,4S)-4-(4-hydroxy-3-methoxy-phenyl)-7-methoxy-2,3-dimethylol-tetralin-6-ol	66.51047	360.44	0.38869	Forsythia suspensa
81	MOL003290	(3R,4R)-3,4-bis[(3,4-dimethoxyphenyl) methyl]oxolan-2-one	52.30461	386.48	0.4849	Forsythia suspensa
82	MOL003281	20(S)-dammar-24-ene-3β,20-diol-3-acetate	40.23	486.86	0.82116	Forsythia suspensa
83	MOL003315	3beta-Acetyl-20,25-epoxydammarane-24alpha-ol	33.06511	502.86	0.79318	Forsythia suspensa
84	MOL003306	ACon1_001697	85.11772	372.45	0.56703	Forsythia suspensa
85	MOL003348	adhyperforin	44.03419	550.9	0.61329	Forsythia suspensa
86	MOL000522	arctiin	34.44847	534.61	0.84109	Forsythia suspensa
87	MOL000791	bicuculline	69.66746	367.38	0.88223	Forsythia suspensa
88	MOL003322	FORSYTHINOL	81.2475	372.45	0.56646	Forsythia suspensa
89	MOL003347	hyperforin	44.03317	536.87	0.598	Forsythia suspensa
90	MOL003365	Lactucasterol	40.99114	426.75	0.84862	Forsythia suspensa
91	MOL003370	Onjixanthone I	79.15712	302.3	0.29993	Forsythia suspensa
92	MOL003305	PHILLYRIN	36.39569	534.61	0.86315	Forsythia suspensa
93	MOL003344	β-amyrin acetate	42.06007	468.84	0.74022	Forsythia suspensa
94	MOL000173	wogonin	30.68457	284.28	0.22942	Forsythia suspensa, Cortex dictamni
95	MOL000211	Mairin	55.37707	456.78	0.7761	Forsythia suspensa, Radix glycyrrhizae, Paeoniae Radix Alba, Cortex moutan
96	MOL001919	(3S,5R,8R,9R,10S,14S)-3,17-dihydroxy-4,4,8,10,14-pentamethyl-2,3,5,6,7,9-hexahydro-1H-cyclopenta[a]phenanthrene-15,16-dione	43.5562	358.52	0.53276	Paeoniae Radix Alba
97	MOL001910	11alpha,12alpha-epoxy-3beta-23-dihydroxy-30-norolean-20-en-28,12beta-olide	64.77389	470.71	0.37586	Paeoniae Radix Alba
98	MOL001928	albiflorin_qt	66.64077	318.35	0.32626	Paeoniae Radix Alba
99	MOL001930	benzoyl paeoniflorin	31.27447	584.62	0.74612	Paeoniae Radix Alba
100	MOL001921	Lactiflorin	49.12132	462.49	0.79711	Paeoniae Radix Alba, Radix paeoniae rubrathe
101	MOL001918	paeoniflorgenone	87.59312	318.35	0.36678	Paeoniae Radix Alba, Radix paeoniae rubrathe
102	MOL001924	paeoniflorin	53.87038	480.51	0.78709	Paeoniae Radix Alba, Radix paeoniae rubrathe
103	MOL001925	paeoniflorin_qt	68.17576	318.35	0.39507	Paeoniae Radix Alba, Radix paeoniae rubrathe, Cortex moutan
104	MOL004924	(-)-Medicocarpin	40.99397	432.46	0.95059	Radix glycyrrhizae

105	MOL004941	(2R)-7-hydroxy-2-(4-hydroxyphenyl) chroman-4-one	71.12299	256.27	0.18303	Radix glycyrrhizae
106	MOL004805	(2S)-2-[4-hydroxy-3-(3-methylbut-2-enyl) phenyl]-8,8-dimethyl-2,3-dihydropyrano[2,3-f]chromen-4-one	31.78703	390.51	0.72403	Radix glycyrrhizae
107	MOL004824	(2S)-6-(2,4-dihydroxyphenyl)-2-(2-hydroxypropan-2-yl)-4-methoxy-2,3-dihydrofuro[3,2-g] chromen-7-one	60.25041	384.41	0.63433	Radix glycyrrhizae
108	MOL004945	(2S)-7-hydroxy-2-(4-hydroxyphenyl)-8-(3-methylbut-2-enyl)chroman-4-one	36.56537	324.4	0.32291	Radix glycyrrhizae
109	MOL004815	(E)-1-(2,4-dihydroxyphenyl)-3-(2,2-dimethylchromen-6-yl)prop-2-en-1-one	39.61686	322.38	0.35077	Radix glycyrrhizae
110	MOL004898	(E)-3-[3,4-dihydroxy-5-(3-methylbut-2-enyl) phenyl]-1-(2,4-dihydroxyphenyl)prop-2-en-1-one	46.26792	340.4	0.3062	Radix glycyrrhizae
111	MOL004914	1,3-dihydroxy-8,9-dimethoxy-6-benzofurano[3,2-c]chromenone	62.90135	328.29	0.52759	Radix glycyrrhizae
112	MOL004913	1,3-dihydroxy-9-methoxy-6-benzofurano[3,2-c]chromenone	48.14154	298.26	0.42831	Radix glycyrrhizae
113	MOL005013	18α-hydroxyglycyrrhetic acid	41.16139	486.76	0.7091	Radix glycyrrhizae
114	MOL004959	1-Methoxyphaseollidin	69.98098	354.43	0.63739	Radix glycyrrhizae
115	MOL004866	2-(3,4-dihydroxyphenyl)-5,7-dihydroxy-6-(3-methylbut-2-enyl)chromone	44.15196	354.38	0.41482	Radix glycyrrhizae
116	MOL004978	2-[(3R)-8,8-dimethyl-3,4-dihydro-2H-pyrano[6,5-f]chromen-3-yl]-5-methoxyphenol	36.21429	338.43	0.52122	Radix glycyrrhizae
117	MOL004849	3-(2,4-dihydroxyphenyl)-8-(1,1-dimethylprop-2-enyl)-7-hydroxy-5-methoxy-coumarin	59.62247	368.41	0.42894	Radix glycyrrhizae
118	MOL004863	3-(3,4-dihydroxyphenyl)-5,7-dihydroxy-8-(3-methylbut-2-enyl)chromone	66.37125	354.38	0.41392	Radix glycyrrhizae
119	MOL004905	3,22-Dihydroxy-11-oxo-delta(12)-oleanene-27-alpha-methoxycarbonyl-29-oic acid	34.31942	512.75	0.54718	Radix glycyrrhizae
120	MOL004966	3'-Hydroxy-4'-O-Methylglabridin	43.71495	354.43	0.57406	Radix glycyrrhizae
121	MOL004974	3'-Methoxyglabridin	46.16151	354.43	0.57393	Radix glycyrrhizae
122	MOL004864	5,7-dihydroxy-3-(4-methoxyphenyl)-8-(3-methylbut-2-enyl)chromone	30.48878	352.41	0.41002	Radix glycyrrhizae
123	MOL004989	6-prenylated eriodictyol	39.22383	356.4	0.41259	Radix glycyrrhizae
124	MOL004990	7,2',4'-trihydroxy-5-methoxy-3-arylcoumarin	83.71437	300.28	0.27136	Radix glycyrrhizae
125	MOL004991	7-Acetoxy-2-methylisoflavone	38.92333	294.32	0.26217	Radix glycyrrhizae
126	MOL003896	7-Methoxy-2-methyl isoflavone	42.56474	266.31	0.19946	Radix glycyrrhizae
127	MOL004838	8-(6-hydroxy-2-benzofuranyl)-2,2-dimethyl-5-chromenol	58.43728	308.35	0.38106	Radix glycyrrhizae
128	MOL004993	8-prenylated eriodictyol	53.79476	356.4	0.40383	Radix glycyrrhizae
129	MOL000417	Calycosin	47.75183	284.28	0.24278	Radix glycyrrhizae
130	MOL005020	dehydroglyasperins C	53.82326	340.4	0.37006	Radix glycyrrhizae
131	MOL001792	DFV	32.76272	256.27	0.18316	Radix glycyrrhizae
132	MOL004806	euchrenone	30.28726	406.56	0.57386	Radix glycyrrhizae
133	MOL004915	Eurycarpin A	43.27728	338.38	0.37429	Radix glycyrrhizae
134	MOL000392	formononetin	69.67388	268.28	0.21202	Radix glycyrrhizae
135	MOL004996	gadelaidic acid	30.70294	310.58	0.19725	Radix glycyrrhizae
136	MOL004856	Gancaonin A	51.07519	352.41	0.40378	Radix glycyrrhizae
137	MOL004857	Gancaonin B	48.7944	368.41	0.44924	Radix glycyrrhizae
138	MOL005000	Gancaonin G	60.43521	352.41	0.39404	Radix glycyrrhizae
139	MOL005001	Gancaonin H	50.10372	420.49	0.78416	Radix glycyrrhizae
140	MOL004910	Glabranin	52.89566	324.4	0.31208	Radix glycyrrhizae
141	MOL004911	Glabrene	46.26686	322.38	0.43902	Radix glycyrrhizae
142	MOL004908	Glabridin	53.24514	324.4	0.46967	Radix glycyrrhizae

143	MOL004912	Glabrone	52.51217	336.36	0.49645	Radix glycyrrhizae
144	MOL004828	Glepidotin A	44.72187	338.38	0.34685	Radix glycyrrhizae
145	MOL004829	Glepidotin B	64.46292	340.4	0.34485	Radix glycyrrhizae
146	MOL004808	glyasperin B	65.22439	370.43	0.43851	Radix glycyrrhizae
147	MOL004811	Glyasperin C	45.56381	356.45	0.39947	Radix glycyrrhizae
148	MOL004810	glyasperin F	75.8368	354.38	0.53514	Radix glycyrrhizae
149	MOL005007	Glyasperins M	72.67081	368.41	0.59274	Radix glycyrrhizae
150	MOL004879	Glycyrin	52.60657	382.44	0.47466	Radix glycyrrhizae
151	MOL002311	Glycyrol	90.77578	366.39	0.66819	Radix glycyrrhizae
152	MOL004917	glycyroside	37.25032	562.57	0.79156	Radix glycyrrhizae
153	MOL005008	Glycyrrhiza flavonol A	41.27528	370.38	0.59512	Radix glycyrrhizae
154	MOL004835	Glypallichalcone	61.59706	284.33	0.18993	Radix glycyrrhizae
155	MOL004907	Glyzaglabrin	61.06889	298.26	0.35347	Radix glycyrrhizae
156	MOL004957	HMO	38.36542	268.28	0.21067	Radix glycyrrhizae
157	MOL004985	icos-5-enoic acid	30.70294	310.58	0.19725	Radix glycyrrhizae
158	MOL001484	Inermine	75.18306	284.28	0.53754	Radix glycyrrhizae
159	MOL004980	Inflacoumarin A	39.7091	322.38	0.32613	Radix glycyrrhizae
160	MOL004948	Isoglycyrol	44.69923	366.39	0.83845	Radix glycyrrhizae
161	MOL004949	Isolicoflavonol	45.16999	354.38	0.41859	Radix glycyrrhizae
162	MOL000354	isorhamnetin	49.60438	316.28	0.306	Radix glycyrrhizae
163	MOL004814	Isotrifoliol	31.94479	298.26	0.42422	Radix glycyrrhizae
164	MOL000239	Jaranol	50.82882	314.31	0.29148	Radix glycyrrhizae
165	MOL004988	Kanzonol F	32.46833	420.54	0.89364	Radix glycyrrhizae
166	MOL004820	kanzonols W	50.48008	336.36	0.51704	Radix glycyrrhizae
167	MOL005003	Licoagrocarpin	58.8139	338.43	0.58498	Radix glycyrrhizae
168	MOL005012	Licoagroisoflavone	57.28224	336.36	0.48679	Radix glycyrrhizae
169	MOL000497	licochalcone a	40.78965	338.43	0.28517	Radix glycyrrhizae
170	MOL004841	Licochalcone B	76.75735	286.3	0.1935	Radix glycyrrhizae
171	MOL004848	licochalcone G	49.25496	354.43	0.32325	Radix glycyrrhizae
172	MOL004882	Licocoumarone	33.21085	340.4	0.3568	Radix glycyrrhizae
173	MOL004885	licoisoflavanone	52.46625	354.38	0.54488	Radix glycyrrhizae
174	MOL004883	Licoisoflavone	41.61022	354.38	0.41646	Radix glycyrrhizae
175	MOL004884	Licoisoflavone B	38.92871	352.36	0.54714	Radix glycyrrhizae
176	MOL004904	licopyranocoumarin	80.36001	384.41	0.6535	Radix glycyrrhizae
177	MOL004860	licorice glycoside E	32.88743	693.71	0.27218	Radix glycyrrhizae
178	MOL004855	Licoricone	63.57846	382.44	0.4712	Radix glycyrrhizae
179	MOL004903	liquiritin	65.69011	418.43	0.73893	Radix glycyrrhizae
180	MOL003656	Lupiwighteone	51.63569	338.38	0.36739	Radix glycyrrhizae
181	MOL002565	Medicarpin	49.21982	270.3	0.3351	Radix glycyrrhizae
182	MOL005016	Odoratin	49.94822	314.31	0.30487	Radix glycyrrhizae
183	MOL005017	Phaseol	78.76622	336.36	0.57867	Radix glycyrrhizae
184	MOL004833	Phaseolinisoflavan	32.00811	324.4	0.44538	Radix glycyrrhizae
185	MOL004961	Quercetin der.	46.44939	330.31	0.3343	Radix glycyrrhizae
186	MOL004827	Semilicoisoflavone B	48.77755	352.36	0.54732	Radix glycyrrhizae
187	MOL004891	shinpterocarpin	80.29528	322.38	0.72746	Radix glycyrrhizae
188	MOL004935	Sigmoidin-B	34.88109	356.4	0.41455	Radix glycyrrhizae
189	MOL000500	Vestitol	74.65519	272.32	0.20935	Radix glycyrrhizae
190	MOL005018	Xambioona	54.84916	388.49	0.87419	Radix glycyrrhizae
191	MOL013129	(2R,3R)-2-(3,5-dihydroxyphenyl)-3,5,7-trihydroxychroman-4-one	63.17278	304.27	0.27209	Rhizoma smilacis glabrae
192	MOL013117	4,7-Dihydroxy-5-methoxyl-6-methyl-8-formyl-flavan	37.03309	314.36	0.27872	Rhizoma smilacis glabrae
193	MOL004575	astilbin	36.46196	450.43	0.73628	Rhizoma smilacis glabrae

194	MOL004580	cis-Dihydroquercetin	66.437	304.27	0.27344	Rhizoma smilacis glabrae
195	MOL000546	diosgenin	80.87792	414.69	0.80979	Rhizoma smilacis glabrae
196	MOL013119	Enhydrin	40.56299	464.51	0.73615	Rhizoma smilacis glabrae
197	MOL004567	isoengelitin	34.65054	434.43	0.69535	Rhizoma smilacis glabrae
198	MOL013118	Neoastilbin	40.54338	450.43	0.7363	Rhizoma smilacis glabrae
199	MOL001736	(-)-taxifolin	60.50622	304.27	0.27342	Rhizoma smilacis glabrae, Cassia twig
200	MOL004576	taxifolin	57.84156	304.27	0.27345	Rhizoma smilacis glabrae, Cassia twig
201	MOL000359	sitosterol	36.91391	414.79	0.7512	Rhizoma smilacis glabrae, Paeoniae Radix Alba, Cassia twig, Radix glycyrrhizae, Cortex moutan, Radix paeoniae rubrathe
202	MOL004328	naringenin	59.2939	272.27	0.21128	Rhizoma smilacis glabrae, Radix glycyrrhizae
203	MOL002086	1-[(5R,8R,9S,10S,12R,13S,14S,17S)-12-hydroxy-10,13-dimethyl-2,3,4,5,6,7,8,9,11,12,14,15,16,17-tetradecahydro-1H-cyclopenta [a] phenanthren-17-yl]ethanone	33.47418	318.55	0.42108	Radix Aconiti Preparata
204	MOL002087	delta4,16-Androstadien-3-one	37.62877	270.45	0.30611	Radix Aconiti Preparata
205	MOL000538	hypaconitine	31.38846	615.79	0.26085	Radix Aconiti Preparata

Supplementary Table 2. Disease targets of transcriptomics based on GEO database

No.	Symbol	Description	GIFtS	GC ID	Score
1	BTG2	BTG Anti-Proliferation Factor 2	45	GC01P203305	49.14
2	IGHM	Immunoglobulin Heavy Constant Mu	40	GC14M113841	47.02
3	DDX3Y	DEAD-Box Helicase 3 Y-Linked	45	GC0YP012903	39.04
4	MIR8071-2///MIR8071-1	MicroRNA 8071-2	8	GC14P105640	14.8
5	ELL2	Elongation Factor For RNA Polymerase II 2	46	GC05M095885	51.09
6	RTN1	Reticulon 1	45	GC14M059595	42.78
7	RGS16	Regulator Of G Protein Signaling 16	46	GC01M182598	45.03
8	SNORD10///SNORA48/// SNORA67///EIF4A1	Small Nucleolar RNA, C/D Box 10	18	GC17P012064	28.89
9	MYC	MYC Proto-Oncogene, BHLH Transcription Factor	59	GC08P127735	146.34
10	JCHAIN	Joining Chain Of Multimeric IgA And IgM	44	GC04M070655	27.74
11	ATF3	Activating Transcription Factor 3	51	GC01P212565	58.79
12	ACACB	Acetyl-CoA Carboxylase Beta	52	GC12P109116	40.83
13	TRAV20	T Cell Receptor Alpha Variable 20	18	GC14P036108	18.34
14	LOC100509457///HLA-DQA2///HLA-DQA1	Major Histocompatibility Complex, Class II, DQ Alpha 2	43	GC06P032741	31.03
15	RND1	Rho Family GTPase 1	42	GC12M048857	37.57
16	SEL1L3	SEL1L Family Member 3	41	GC04M025715	32.36
17	BLNK	B Cell Linker	53	GC10M096264	54.63
18	TCF7L2	Transcription Factor 7 Like 2	53	GC10P112950	86.29
19	IGHG1	Immunoglobulin Heavy Constant Gamma 1 (G1m Marker)	40	GC14M105736	32.01
20	FOXO3	Forkhead Box O3	53	GC06P108559	63.38
21	GADD45B	Growth Arrest And DNA Damage Inducible Beta	43	GC19P002476	34.8
22	IGLV1-44	Immunoglobulin Lambda Variable 1-44	22	GC22P046894	17.25

23	MYH11	Myosin Heavy Chain 11	52	GC16M016034	57.54
24	GM2A	Ganglioside GM2 Activator	50	GC05P151212	39.23
25	IGLJ3	Immunoglobulin Lambda Joining 3	15	GC22P046942	15.42
26	ZFP36L2	ZFP36 Ring Finger Protein Like 2	44	GC02M043184	45.89
27	CDKN1A	Cyclin Dependent Kinase Inhibitor 1A	55	GC06P096237	54.82
28	YME1L1	YME1 Like 1 ATPase	50	GC10M027110	42.11
29	ITGA4	Integrin Subunit Alpha 4	55	GC02P181456	50.29
30	TRAJ17	T Cell Receptor Alpha Joining 17	15	GC14P036198	14.13
31	LCK	LCK Proto-Oncogene, Src Family Tyrosine Kinase	59	GC01P032251	115
32	LOC101060835///HLA-DQB1	Major Histocompatibility Complex, Class II, DQ Beta 1	48	GC06M074984	71.43
33	MGC40069	hypothetical protein MGC40069			
34	FOSB	FosB Proto-Oncogene, AP-1 Transcription Factor Subunit	49	GC19P045467	62.04
35	CXCL13	C-X-C Motif Chemokine Ligand 13	47	GC04P077511	56.83
36	CKAP2	Cytoskeleton Associated Protein 2	44	GC13P052455	40
37	PLAAT4	Phospholipase A And Acyltransferase 4	39	GC11P063792	20.91
38	CD300A	CD300a Molecule	47	GC17P074466	55.9
39	HLA-DPA1	Major Histocompatibility Complex, Class II, DP Alpha 1	48	GC06M033064	45.02
40	CAPG	Capping Actin Protein, Gelsolin Like	48	GC02M085391	47.65
41	FOXO3B	Forkhead Box O3B	20	GC17M053374	24.14
42	ADCY2	Adenylate Cyclase 2	52	GC05P007396	36.81
43	CD2	CD2 Molecule	51	GC01P116754	76.75
44	LRMP///IRAG2///JAW1	Inositol 1,4,5-Triphosphate Receptor Associated 2	39	GC12P025615	26.13
45	CYAT1///IGLV1-44///IGLC1	Immunoglobulin Lambda Light Chain-Like	4	GC22U900796	13.25
46	APOLD1	Apolipoprotein L Domain Containing 1	38	GC12P012725	30.64
47	LAMA4	Laminin Subunit Alpha 4	52	GC06M112107	47.29
48	GAP43	Growth Associated Protein 43	50	GC03P115623	48.02
49	TTC3P1///TTC3	Tetratricopeptide Repeat Domain 3 Pseudogene 1	13	GC0XM075740	16.2
50	TIPARP	TCDD Inducible Poly(ADP-Ribose) Polymerase	40	GC03P156673	49.94
51	FKBP5	FKBP Prolyl Isomerase 5	56	GC06M075061	61.01
52	MLIP	Muscular LMNA Interacting Protein	42	GC06P053929	39.03
53	KLF9	KLF Transcription Factor 9	42	GC09M070384	47.64
54	CCL18	C-C Motif Chemokine Ligand 18	42	GC17P036064	40.29
55	GABARAPL1	GABA Type A Receptor Associated Protein Like 1	47	GC12P010212	35.26
56	MXRA5	Matrix Remodeling Associated 5	39	GC0XM003308	33.19
57	MCL1	MCL1 Apoptosis Regulator, BCL2 Family Member	55	GC01M153178	64.78
58	TRAC	T Cell Receptor Alpha Constant	34	GC14P036196	25.59
59	JUNB	JunB Proto-Oncogene, AP-1 Transcription Factor Subunit	48	GC19P012791	62.46
60	SOCS3	Suppressor Of Cytokine Signaling 3	50	GC17M078356	66.3
61	LRRC15	Leucine Rich Repeat Containing 15	44	GC03M194357	31.34
62	IL1R1	Interleukin 1 Receptor Type 1	53	GC02P102136	47.11
63	ABLIM1	Actin Binding LIM Protein 1	46	GC10M114514	41.03

64	DPT	Dermatopontin	44	GC01M168696	36.85
65	FOSL2	FOS Like 2, AP-1 Transcription Factor Subunit	48	GC02P028392	49.01
66	EGFR	Epidermal Growth Factor Receptor	62	GC07P055019	200.59
67	FNDC4	Fibronectin Type III Domain Containing 4	42	GC02M027491	34.23
68	GRB10	Growth Factor Receptor Bound Protein 10	50	GC07M050590	72.31
69	HAS1	Hyaluronan Synthase 1	44	GC19M074026	38.54
70	SRSF7	Serine And Arginine Rich Splicing Factor 7	47	GC02M038743	33.65
71	IGLC1	Immunoglobulin Lambda Constant 1	29	GC22P022895	16.55
72	IGKC	Immunoglobulin Kappa Constant	39	GC02M091164	27.4
73	ADAM28	ADAM Metallopeptidase Domain 28	48	GC08P024294	44.55
74	NPAS2	Neuronal PAS Domain Protein 2	47	GC02P100820	55.76
75	ADAMDEC1	ADAM Like Decysin 1	44	GC08P024384	37.03
76	SLC16A7	Solute Carrier Family 16 Member 7	50	GC12P059596	39.21
77	KLF6	KLF Transcription Factor 6	50	GC10M003779	66.4
78	ADAMTS1	ADAM Metallopeptidase With Thrombospondin Type 1 Motif 1	52	GC21M026835	50.9
79	VEGFA	Vascular Endothelial Growth Factor A	56	GC06P043770	65.51
80	GPRC5A	G Protein-Coupled Receptor Class C Group 5 Member A	48	GC12P025226	42.8
81	MAFF	MAF BZIP Transcription Factor F	46	GC22P038200	43.24
82	CD52	CD52 Molecule	44	GC01P026317	56.8
83	IGHA1	Immunoglobulin Heavy Constant Alpha 1	38	GC14M113835	23.8
84	NR4A1	Nuclear Receptor Subfamily 4 Group A Member 1	54	GC12P052022	44.46
85	LOC100506718///FLRT2	Fibronectin Leucine Rich Transmembrane Protein 2	46	GC14P085530	46.65
86	RHOBTB3	Rho Related BTB Domain Containing 3	44	GC05P095713	42.39
87	PLPP3	Phospholipid Phosphatase 3	47	GC01M056495	34.72
88	MARCKS	Myristoylated Alanine Rich Protein Kinase C Substrate	46	GC06P113857	63.69
89	COL1A1	Collagen Type I Alpha 1 Chain	56	GC17M054676	90.15
90	TRDV2	T Cell Receptor Delta Variable 2	21	GC14P036137	23.41
91	HNRNPUL2-BSCL2///BSCL2	HNRNPUL2-BSCL2 Readthrough (NMD Candidate)	18	GC11M102414	41.07
92	IL32	Interleukin 32	45	GC16P014513	26.87
93	EGR1	Early Growth Response 1	52	GC05P138465	52.92
94	EDNRB	Endothelin Receptor Type B	56	GC13M077895	78.32
95	MAP1B	Microtubule Associated Protein 1B	51	GC05P072107	59.53
96	KMO	Kynurenine 3-Monooxygenase	53	GC01P241532	38.54
97	IGKV1OR2-118	Immunoglobulin Kappa Variable 1/OR2-118 (Pseudogene)	9	GC02M090315	13.25
98	BMS1P20	BMS1 Pseudogene 20	18	GC22P022298	21.84
99	DUSP1	Dual Specificity Phosphatase 1	52	GC05M172768	48.48
100	IGLL3P	Immunoglobulin Lambda Like Polypeptide 3, Pseudogene	14	GC22P025318	13.25
101	BTN3A2	Butyrophilin Subfamily 3 Member A2	43	GC06P026365	28.74
102	IGLV@	Immunoglobulin Lambda Variable Cluster	7	GC22U990033	17.53
103	LDLR	Low Density Lipoprotein Receptor	58	GC19P011091	68
104	JUN	Jun Proto-Oncogene, AP-1 Transcription Factor Subunit	55	GC01M058780	115.26

105	LTA4H	Leukotriene A4 Hydrolase	53	GC12M096000	46.11
106	FKBP11	FKBP Prolyl Isomerase 11	43	GC12M050062	38.14
107	IGK	Immunoglobulin Kappa Locus	19	GC02P088857	25.56
108	CYR61///CCN1///GIG1///IGFBP10	Cellular Communication Network Factor 1	47	GC01P085581	45.89
109	IGLL5	Immunoglobulin Lambda Like Polypeptide 5	36	GC22P046941	23.49
110	IGKV1OR2-108	Immunoglobulin Kappa Variable 1/OR2-108 (Non-Functional)	18	GC02P113406	19.13
111	DDX60	DExD/H-Box Helicase 60	42	GC04M168216	38.01
112	KIF11	Kinesin Family Member 11	56	GC10P092574	47.13
113	GABARAPL3///GABARAPL1	GABA Type A Receptor Associated Protein Like 3 Pseudogene	25	GC15M090346	26.28